Chem Soc Rev

TUTORIAL REVIEW

View Article Online
View Journal

Check for updates

Cite this: DOI: 10.1039/d5cs01539a

Radical-promoted "unstrained" C–C and C–N bond cleavage: a blueprint for deconstructive skeletal editing

José Justicia and Sara P. Morcillo *

Unstrained cyclic scaffolds are commonly regarded as inert backbones; however, recent radical and radical-ion strategies show that their connectivity can be deliberately reprogrammed when appropriate functional gateways are embedded in the ring. This Tutorial Review treats radical-promoted C–C and C–N bond cleavage as a design problem defined by three interdependent elements: the gateway that enables bond scission (alcohols, ketones, and amines), the activation mode that generates oxygen- or nitrogen-centred intermediates (single-electron transfer (SET), proton-coupled electron transfer (PCET), ligand-to-metal charge transfer (LMCT), and electron donor–acceptor (EDA) activation), and the downstream interception that determines whether deconstruction evolves into productive skeletal editing. Rather than compiling reactions, we distil practical rules for aligning activation with radical polarity and lifetime, and show how closely related intermediates can be steered toward ring opening and functionalisation or, under tighter kinetic constraints, toward ring contraction and expansion. Particular emphasis is placed on ketone-derived gateways that channel C–C scission through iminyl radicals or pre-aromatic intermediates, and on the direct use of cyclic alcohols *via* alkoxy radicals, organised through a two-step framework that separates radical generation from the divergent reactivity of the β-scission-derived carbon-centred radical.

Received 23rd December 2025

DOI: 10.1039/d5cs01539a

rsc.li/chem-soc-rev

Open Access Article. Published on 16 June 2026. Downloaded on 6/19/2026 2:50:40 PM.
This article is licensed under a Creative Commons Attribution 3.0 Unported Licence.

Key learning points

(1) Which functional groups allow C–C or C–N bond cleavage in unstrained cyclic systems under radical conditions.
(2) How different activation strategies (SET, PCET, LMCT among others) are used to generate oxygen- and nitrogen-centred radicals from common precursors.
(3) What factors control the fate of the carbon-centred radical after the common ring-opening step, determining whether contraction, expansion, or functionalization occurs.
(4) Why unstrained five- and six-membered rings are particularly difficult to edit, and how current strategies overcome this limitation.
(5) How diverse radical activation strategies converge on a small number of mechanistic bottlenecks in unstrained skeletal editing.

1. Introduction

A central question in modern synthesis is the fate of cyclic scaffolds: to what extent can the connectivity of cyclic scaffolds be modified in a controlled manner? Saturated rings, both carbocycles and N-heterocycles, have long been treated as robust backbones whose unstrained, non-polarised σ bonds are poor targets for selective cleavage. In the absence of ring strain or a polar activating group, there is little driving force for C–C or C–N bond scission, and synthetic efforts have therefore concentrated on peripheral modifications, such as late-stage C(sp^3)–H functionalization, oxidation or alkylation. Skeletal editing challenges this view, questioning whether the backbone of a ring can be reprogrammed and its connectivity redirected without rebuilding the entire framework. As shown in seminal radical and radical-ion studies, once bonds long considered inert are activated, rings become reconfigurable platforms rather than rigid architectures.

Retrosynthetic logic itself shifts from treating the core as fixed to treating it as an editable element.[1] This change enables direct reprogramming of ring connectivity rather than peripheral modification. Why does this matter? In medicinal chemistry, the concept of scaffold hopping describes the redesign of a bioactive molecule by altering its central core while retaining

Department of Organic Chemistry, Faculty of Sciences, Unidad de Excelencia de Química (UEQ), University of Granada, Avda. Fuente Nueva s/n, 18071 Granada, Spain. E-mail: samorcillo@ugr.es

Open Access Article. Published on 16 June 2026. Downloaded on 6/19/2026 2:50:40 PM. This article is licensed under a Creative Commons Attribution 3.0 Unported Licence.

biological function.[1a,2] When this principle is applied in synthetic strategies, yet recognizably derived from familiar scaffolds. Although scaffold hopping and skeletal editing are conceptually distinct, they often converge in practice by modifying the molecular backbone to access new chemical space and reveal hidden structure–activity relationships. Radical-mediated cleavage has been decisive in this transformation.[3] Direct C–C bond scission in carbocycles has opened frameworks that were once inaccessible. Progress in C–N cleavage has followed closely, reshaping privileged N-heterocycles that dominate pharmaceuticals and agrochemicals. Indeed, 88% of FDA-approved small-molecule drugs between 2015 and 2020 contained at least one N-heterocycle[4]—yet until recently, the ring core itself was untouched. Deconstructive strategies now enable nitrogen deletion, oxidative scission, deaminative functionalization, and photomediated contraction, redefining the possible transformations with these scaffolds.[1a,5]

At the mechanistic core lie radical and radical-ion intermediates, most often generated through single-electron transfer (SET). While visible-light photoredox catalysis has become the dominant platform,[6] electrochemistry, photoelectrochemistry, and transition-metal activation also provide powerful alternatives. Within this landscape, several complementary entry modes can be distinguished—proton-coupled electron transfer (PCET),[7] ligand-to-metal charge transfer (LMCT),[8] hydrogen-atom transfer (HAT), halogen-atom transfer (XAT)[9] or electron donor–acceptor (EDA) complexes. Together, these strategies converge on a common outcome: the generation of oxygen- and nitrogen-centred radicals that act as gateways for skeletal reprogramming. Alkoxy radicals promote β-scission of adjacent C–C or C–N bonds, whereas iminyl and aminium radicals enable selective C–C bond cleavage under certain polarity rules.

The synthetic outcome of these processes is dictated by the fate of the radical intermediates formed after bond scission. Three general trajectories can be distinguished in Scheme 1A. Ring contraction compresses the framework into a smaller skeleton and is now accessible even in saturated and heteroatom-containing rings. Ring expansion converts small rings into medium-sized or macrocyclic architectures, although direct expansion through cleavage of unstrained bonds remains uncommon. Ring opening and functionalization, often referred to as deconstruction/functionalisation, generates acyclic intermediates that can be trapped or diversified. Together with ring contraction and expansion, these processes exemplify scaffold hopping: contraction alters polarity and conformational preferences, expansion introduces flexibility and new vectors, and opening reshapes the 3D topology and polarity of the framework. In drug discovery, such transformations promote ring-distortion strategies that expand bioactive chemical space,[10] and in molecular materials[11] they offer orthogonal control over conjugation, rigidity, and optoelectronic response. Scheme 1 summarises these pathways, which are discussed below in terms of how radical intermediates are directed toward opening, contraction, expansion, or selective functionalisation.

This Tutorial does not aim to catalogue all reported examples, as excellent reviews already cover specific activation modes and transformations. Instead, unstrained cyclic systems are treated as reconfigurable platforms, and we analyze how radical deconstruction can be redirected to access new molecular architectures. We aim to identify the key radical gateways, activation principles, and downstream pathways, and to extract practical design rules for skeletal editing. Accordingly, Section 2 introduces the working definitions relevant to bond cleavage and radical reactivity. Section 3 focuses on ring opening followed by functionalization of unstrained cycles. Section 4 examines C–C bond cleavage pathways that enable ring expansion. Finally, Section 5 addresses the more challenging cases of

José Justicia

José Justicia earned his Chemistry degree (1998), MSc (2000), and PhD (2004, recognized among the best theses) at the University of Granada. He completed postdoctoral research at the University of Bonn with Prof. A. Gansauer (2004–2006), focusing on Ti(III)-mediated radical methodologies for terpenoid synthesis. He later returned to Granada under the Juan de la Cierva program and became Associate Professor in Organic Chemistry in 2011. He has authored around 60 publications, supervised six PhD theses, and participated in multiple competitive projects. His research centers on organic synthesis, new synthetic methodologies, photochemically active carbon-based materials, and the total synthesis of bioactive terpenoids.

Sara P. Morcillo

Sara P. Morcillo is Associate Professor of Organic Chemistry at the University of Granada. She obtained her Ph.D. in 2014 working on radical chemistry and functional organic materials (recognized among the best theses). She then carried out postdoctoral research at Université Paris-Saclay (Prof. V. Gandon, 2014–2016) on Ca-, Bi-, and Fe-catalyzed transformations, and at the University of Manchester (Prof. D. Leonori, 2016–2018), developing photoredox methodologies. Her current research focuses on the design of bioinspired rotary molecular systems and chiral switches based on helical structures, including o-OPEs and distorted nanographenes, aimed at modulating chiroptical properties and developing functional organic materials.

This journal is © The Royal Society of Chemistry 2026

Open Access Article. Published on 16 June 2026. Downloaded on 6/19/2026 2:50:40 PM.
This article is licensed under a Creative Commons Attribution 3.0 Unported Licence.

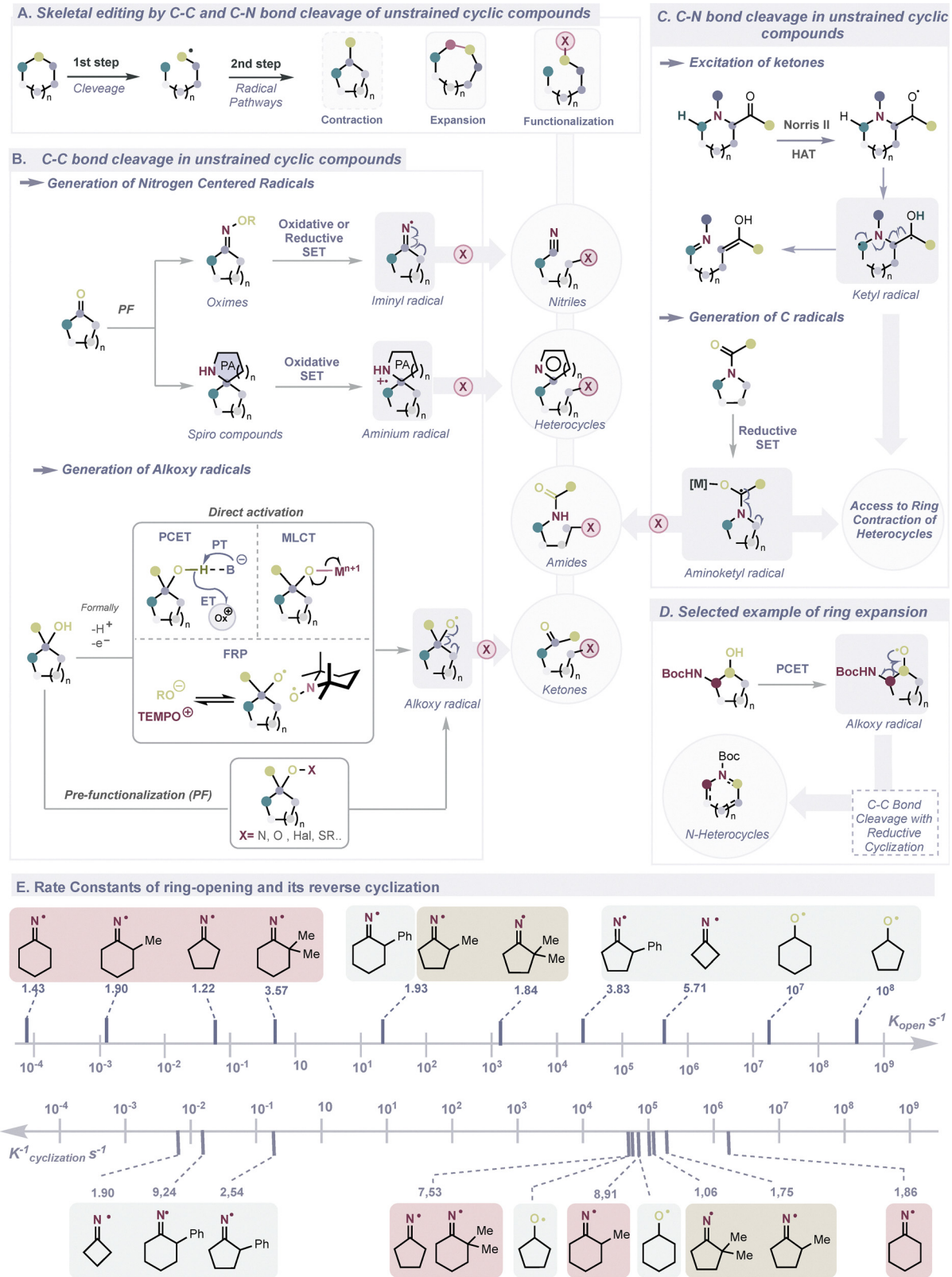

Scheme 1 Summarises of the key concepts in this Tutorial. (A) Radical skeletal editing after C–C or C–N bond cleavage in unstrained cycles. (B) Dominant deconstruction/functionalisation pathways following ring opening. (C) Limited strategies for C–N bond cleavage, including a representative example of ring expansion. (D) Selected example of ring expansion. (E) Kinetic competition between ring opening and ring closure in alkoxy and iminyl radicals.

Open Access Article. Published on 16 June 2026. Downloaded on 6/19/2026 2:50:40 PM. This article is licensed under a Creative Commons Attribution 3.0 Unported Licence.

C–N bond cleavage, where functionalization or ring contraction is only possible when ring reclosure is carefully controlled, which remains the main challenge and opportunity in this field.

2. Functional handles and radical gateways for skeletal editing

General framework: which rings can be deconstructed?

A survey of successful cases reveals a pattern: most involve all-carbon cycles carrying an alcohol or a ketone, or alternatively, N-heterocyclic. These functional groups act as radical gateways, but their behavior differs. Ring fragmentations are particularly illustrative, as they unmask latent functional groups and generate two functional handles defined by ring size. Unlike C–H functionalisation, which decorates the periphery, these deconstructive events inherently reshape the molecular backbone. The scope of this strategy depends critically on the functional groups embedded within the ring, which serve as radical gateways. Among the most prominent gateways are cyclic alcohols, ketones, and amines, with distinct challenges and opportunities for productive bond scission (see Scheme 1B). In this sense, cyclic alcohols can undergo direct deconstruction *via* alkoxy radicals, in which β-scission reveals a ketone fragment that was latent in the cyclic structure. Cyclic ketones, by contrast, are far less straightforward. Direct ring opening would generate an acylium intermediate, a highly reactive species that is difficult to capture productively. For this reason, ketones are usually derivatised into oximes, precursors of iminyl radicals, whose fragmentation reveals nitriles as the latent functional group. Alternatively, condensation into pre-aromatic intermediates (PAIs) channels scission into heteroaromatic scaffolds effectively, unmasking aromatic frameworks. A particularly elegant solution is exemplified by the Interrupted Dowd–Beckwith (IDB) reaction, which achieves direct deconstruction of cyclic ketones *via* acylium intermediates, and channels these otherwise unstable species into productive functionalisation.[12] N-heterocyclic compounds represent a third class of gateway, but their direct fragmentation is rare. In unstrained systems, C–N bond homolysis lacks an intrinsic driving force (see Scheme 1C and D). Success has come when scission is coupled to a strong bias, such as the formation of ketyl or aminoketyl radicals (Scheme 1C), or alignment with aromatization in PAIs (Scheme 1D). These strategies explain both why amines are less frequently represented and where new opportunities may lie.

The take-home message is that skeletal editing does not begin from an inert ring, but from functional groups that can serve as gateways, and from an understanding of the driving forces—β-scission, aromatization, or ketyl stabilization—that make bond cleavage viable.[12] These bases will guide the following sections, which analyze how the radical intermediates accessed through these gateways lead to divergent trajectories of ring opening, contraction, and expansion reactions.

2.1. Radical gateways for C–C bond cleavage

Three radical gateways dominate C–C bond scission in unstrained carbocycles: alkoxy, iminyl, and aminium radicals. Each embodies a different electronic structure—nucleophilic, ambiphilic, or electrophilic—that governs both selectivity and outcome.

Iminyl radicals[13]. These σ-radicals, arising from sp^2-hybridised nitrogen in oximes, undergo β-scission of adjacent C–C bonds to yield alkylnitriles, highly valued across medicinal and natural product chemistry. Their generation is facilitated by the relatively weak N–O bond (BDE $\approx$ 50 kcal mol^{-1}), accessible through thermal, photochemical, or SET-based activation. The abundance of ketone precursors and the privileged status of nitrile products explain the prominence of this gateway.

Aminium radicals. Generated by SET oxidation of N-heterocyclic or PAIs, these electrophilic π-radicals fragment when scission is coupled to aromatization. This alignment with thermodynamic bias channels deconstruction, yielding quinazolinones.[14]

Alkoxy radicals. Oxygen-centred radicals remain the most established entry point into C–C bond cleavage.[15] Their intrinsic predisposition for β-fragmentation ensures that, once embedded in a ring, adjacent C–C bonds are primed to rupture. The challenge lies in their direct generation from alcohols: O–H bonds (BDE $\approx$ 105 kcal mol^{-1}) are much stronger than those of peroxides or oximes, and alcohols are difficult to oxidise by SET. Recent strategies have overcome these barriers,[16] including PCET (concerted $H^{\bullet}$ removal *via* photoexcited oxidant + base), LMCT (photoexcitation of metal–alkoxides leading to selective M–O homolysis), and frustrated radical pairs (cooperative, non-classical H-atom abstraction). Classical approaches based on N–O or O–O precursors remain widely used but require derivatization.

Kinetic benchmarks. Scheme 1E highlights the kinetic predisposition of alkoxy radicals: β-scission in cycloalkoxy radicals proceeds at $k_{open} \approx 10^8$ s^{-1} (five-membered) and 10^7 s^{-1} (six-membered), while back-closure occurs 3–4 orders of magnitude slower.[17] These values indicate that ring opening is kinetically facile once an alkoxy radical is generated. In addition, overall success also depends on thermodynamics. Small rings such as cyclopropane and cyclobutane carry high strain energies ($\approx$ 27 and 26 kcal mol^{-1}, respectively), so scission is strongly favored by strain release. Medium rings such as cycloheptane and cyclooctane also benefit from the relief of transannular interactions. By contrast, five- and six-membered rings sit at the bottom of the strain-energy curve ($\approx$6 and 0 kcal mol^{-1}, respectively), meaning that bond cleavage provides little or no thermodynamic driving force. As a result, these rings are particularly difficult to fragment productively. The ring opening is kinetically fast, but reclosure competes strongly unless an additional bias is introduced, such as stabilizing substituents, polarity effects, or immediate trapping. Cycloiminyl radicals illustrate this balance. In the absence of bias, they reclose rapidly, but α-phenyl substitution or strain release strongly favours ring opening. As demonstrated in a 2017 study by some of us, α-phenyl groups promote productive scission in both five- and six-membered systems. In contrast, α-methyl or α-H substitution shifts the equilibrium back toward closure.[18] These

 This journal is © The Royal Society of Chemistry 2026

Open Access Article. Published on 16 June 2026. Downloaded on 6/19/2026 2:50:40 PM. This article is licensed under a Creative Commons Attribution 3.0 Unported Licence.

trends rationalize the prevalence of α-phenyl cases and highlight the principle that effective skeletal editing requires coupling kinetic predisposition with a thermodynamic incentive for the open form.

2.2. Radical gateways for C–N bond cleavage

Compared with C–C scission, direct C–N bond cleavage in unstrained rings is less developed but has gained attention as a complementary pathway. Historically, this space was dominated by two-electron transition-metal catalysis.[19] Radical-based strategies now enable homolytic C–N fragmentation and open new trajectories inaccessible to polar mechanisms.[20] One approach involves SET reduction of amides, generating aminoketyl radicals that undergo β-scission of adjacent C–N bonds, selectively opening rings under photoredox conditions in combination with Lewis acids, as depicted in Scheme 1C.[21] Another strategy involves excited-state carbonyl fragmentation, where photoexcitation of cyclic amines with carbonyl substituents initiates Norrish-type cascades (Norrish–II, 1,5-HAT, α-cleavage) that drive selective scission.[5c]

2.3. Polarity, activation, and trapping as unifying principles

Radical behavior follows polarity rules rather than randomness: nucleophilic radicals preferentially react with electrophiles, whereas electrophilic radicals target nucleophiles. The SOMO energy provides a practical descriptor of this ''radical electronegativity''. After bond scission, the fate of the radical depends on interception. Intermediates can be trapped by SOMOphiles (X) through homolytic atom/group transfer (*e.g.*, SH_2 reactions with polarized X–Y bonds), added to activated alkenes in Giese-type processes, or converted into ionic species *via* radical–polar crossover (RPC) to enter polar chemistry. Equally important is how the radical is generated. SET oxidation or reduction, PCET, LMCT, or EDA activation not only produce radicals, but also define their lifetime, polarity, and compatibility with subsequent steps. Productive skeletal editing requires matching radical generation, interception, and catalyst turnover. In some cases, this balance is only achieved by dual catalysis—for example, a photoredox cycle generating radicals that are captured by a transition-metal catalyst in cross-coupling.

Take-home message. Successful skeletal editing requires that the gateway, activation, and trapping steps are properly aligned, ensuring that radical formation, reactivity, and catalytic turnover proceed coherently. The following sections illustrate these principles through representative radical gateways and their distinct outcomes.

3. C–C bond cleavage: deconstructive functionalization

This section provides a global perspective on how unstrained cyclic systems can be opened and selectively functionalised through deconstructive functionalization, with the aim of extracting guiding principles rather than compiling an exhaustive set of examples. We focus on radical gateways and activation modes that unlock C–C scission in the context of skeletal editing. Specifically, we discuss iminyl radicals generated from cyclic ketones *via* oxime derivatives (Section 3.1), aminium radicals accessed from spirocyclic systems derived from cyclic ketones or cyclic amines (Section 3.2), and alkoxy radicals derived from cyclic alcohols (Section 3.3). Because ketones, amines, and alcohols are ubiquitous in natural products and prevalent in drug scaffolds, these entry points are strategically positioned for late-stage modification and scaffold diversification.

3.1. Iminyl radical: deconstructive functionalization of cycloketoxime derivatives

The chemistry of iminyl radicals has evolved from mechanistic curiosity into a versatile platform for molecular deconstruction/functionalization.[22] Their hallmark is the β-scission of the α C–C bond to nitrogen, which consistently releases a nitrile as a stable fragment together with an alkyl radical as the reactive intermediate. Nitriles act both as robust endpoints and as versatile ''handles'' in chemistry and materials science.[23] Their relevance is evident both at the industrial level—acrylonitrile is produced on the million-ton scale[24]—and in pharmaceuticals, where nitrile-containing drugs, such as vildagliptin, reach annual sales above one billion dollars.[25] Oxime derivatives are the most common precursors, since they are easily prepared from cyclic ketones and their relatively weak N–O bond [BDE $\approx$ 50 kcal mol^{-1}] allows homolysis under mild conditions.[26] Alongside photoredox and redox-based strategies—the focus of this section—other activation modes have been reported. For example, Castle *et al.* showed that microwave heating at $\approx$ 90 °C can promote direct N–O scission,[27] while Guo *et al.* described a transition-metal-free deconstruction/borylation of cycloketoxime esters, where DMA coordinates with $B_2(OH)_4$ to generate boryl radicals that trigger N–O homolysis.[28] Further alternatives include the dehydroxylation of neutral oximes and the SET-induced cleavage of *N*-substituted pyridinium salts.[29]

A central guiding principle is redox matching (Scheme 2, panels A/C). By comparing the redox potential of the oxime precursor with that of the photocatalyst,[30] it is possible to predict whether SET will occur and whether the process will follow a reductive or oxidative pathway. This initial step dictates how electron balance is restored and, in turn, which functionalization become accessible after formation of the **alkyl radical B** from **iminyl radical A**. On this basis, we organize the discussion as follows: (i) generation of **A** *via* reductive (Section 3.1.1) or oxidative (Section 3.1.2) SET pathways, (ii) historical developments that optimised these activation modes, and (iii) the divergent reactivity of **B** (Scheme 2, panel D).

SET reduction pathways. In reductive SET manifolds, oxime derivatives act as redox-active esters or ethers. Electron uptake occurs into the N–O fragment, and the nature of the *O*-substituent (aryl, acyl, *etc.*) tunes the reduction potential while dictating the leaving group ability upon bond cleavage. The resulting radical anion undergoes bond cleavage to release

Open Access Article. Published on 16 June 2026. Downloaded on 6/19/2026 2:50:40 PM.
This article is licensed under a Creative Commons Attribution 3.0 Unported Licence.

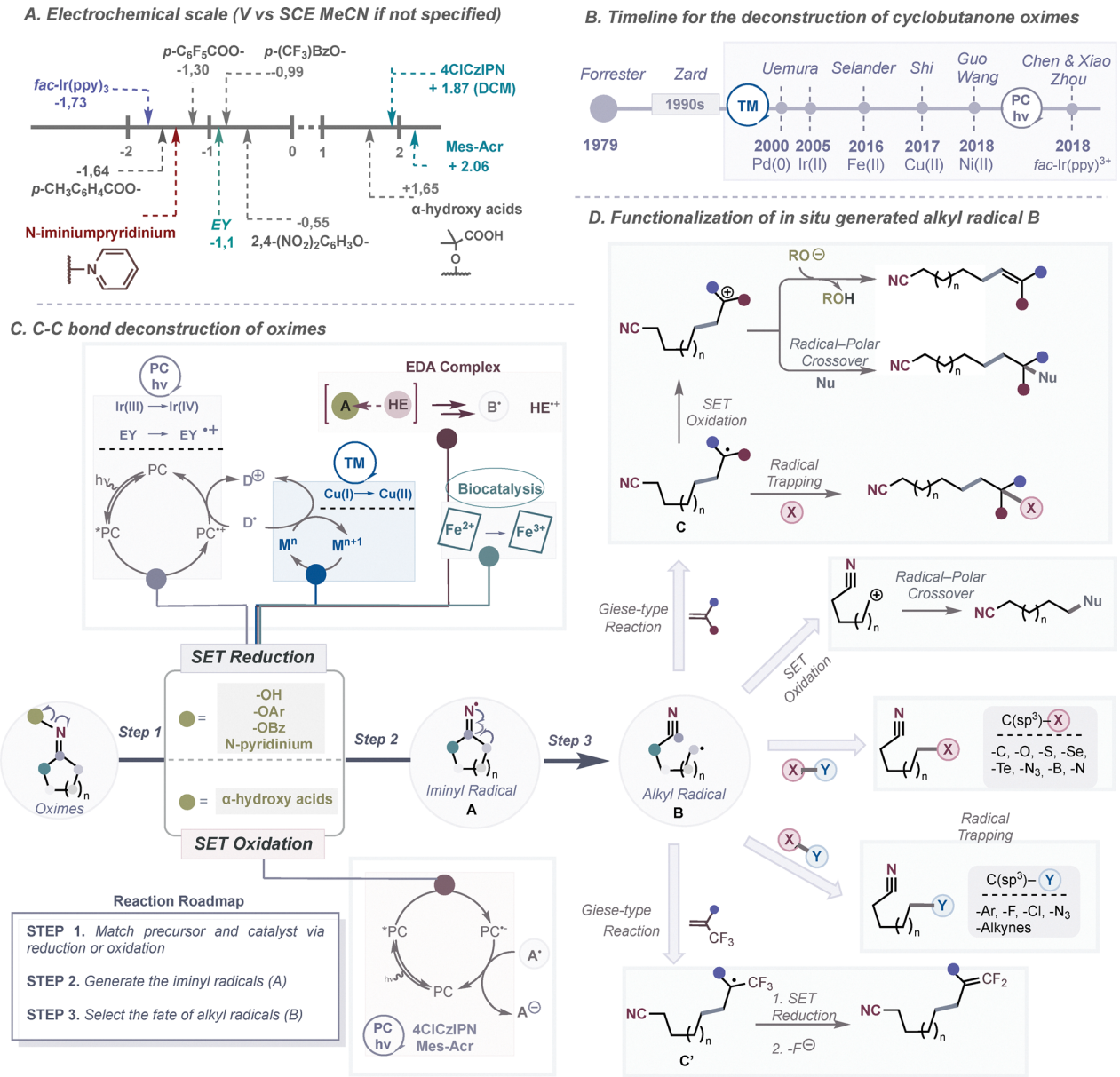

Scheme 2 Deconstruction of oxime derivatives *via* iminyl radicals. (A) Redox potentials of representative oxime precursors and photocatalysts in MeCN (*vs.* SCE), defining accessible SET-reductive and SET-oxidative pathways. (B) Key milestones in the development of cyclobutanone oxime deconstruction from early thermal and metal-catalysed methods to visible-light photoredox strategies. (C) SET-mediated N–O bond cleavage of oxime derivatives (photoredox, metal catalysis, and EDA complexes) generating **iminyl radical A**, followed by β-scission to **alkyl radical B**. (D) Representative reaction manifolds of **alkyl radical B** after deconstruction, including Giese-type addition, radical–polar crossover, SOMOphile trapping, and oxidative group-transfer processes.

the iminy radical. Two families of precursors illustrate this behavior. *O*-Aryl oxime ethers ($R_2C{=}NOAr$) span a broad reduction window (≈ −0.55 to −1.88 V *vs.* SCE), with potentials strongly influenced by aryl substituents and leaving groups.[31] *O*-Acyl oxime esters ($R_2C{=}NO{-}COR'$) display narrower but tuneable windows; for example, cyclobutanone *O*-(*p*-CF_3-benzoyl) oxime reduces at ≈ −0.99 V *vs.* SCE.[32] These values align with common photocatalysts such as $Ir(ppy)_3$ [E^* ≈ −1.73 V *vs.* SCE for $Ir^{III}*/Ir^{IV}$], Cu(I) complexes −1.0 to −1.3 V *vs.* SCE), and eosin Y [E^* ≈ −1.11 V *vs.* SCE for $EY*/EY^{\bullet-}$] (Scheme 2, panel A). Beyond photoredox and transition-metal catalysis, SET reduction can also proceed *via* EDA complexes. Cyclobutanone oxime esters, often bearing *p*-$CF_3C_6H_4COO$ groups, can form EDA assemblies with donors such as DABCO,[33] NHC/Lewis acid systems that generate Breslow enolates,[34] or thiophenolate anions.[35] Upon irradiation, these assemblies undergo SET to release benzoate, the **iminyl radical A**, and a donor-derived radical ($DABCO^{\bullet+}$, $NHC^{\bullet+}$, or $ArS^{\bullet}$) (see Scheme 2). While efficient for strained cyclobutanones, extending this approach to unstrained systems remains challenging.

This journal is © The Royal Society of Chemistry 2026

Open Access Article. Published on 16 June 2026. Downloaded on 6/19/2026 2:50:40 PM. This article is licensed under a Creative Commons Attribution 3.0 Unported Licence.

Combining EDA with Hantzsch ester (HE) as photoactive donor/H-source is emerging as a practical solution (see below and Scheme 2, panel C). In this sense, generating **A** from neutral oximes (non-activated oximes (R = H)) is demanding since their lower redox activity and O–H cleavage compete with N–O scission. Nonetheless, a recent Fe(II)-based biocatalyst enables dehydroxylation,[36] and *N*-iminopyridinium salts offer complementary SET entries.[29b,29c]

SET oxidation pathways. Oxidative SET follows an inverted polarity logic. α-*N*-oxyacids undergo oxidation at the carboxylate, triggering two β-scissions that release the **iminyl radical A**. More generally, deprotonation lowers the oxidation threshold, enabling oxime carboxylates from α-hydroxy acid derivatives to engage with strong photooxidants such as 4CzIPN [E^* ≈ +1.87 (DCM) V *vs*. SCE for 4CzIPN*/4CzIPN$^{\bullet-}$], [Ir(dF(CF$_3$)ppy)$_2$(dtbbpy)]PF$_6$ [E^* ≈ +1.21 V *vs*. SCE for Ir^{III}*/Ir^{II}], or Mes-Acr$^+$ [E^* ≈ +2.06 V *vs*. SCE for Mes-Acr$^+$*/Mes-Acr$^\bullet$] (Scheme 2, panel A).

Historical development. Early contributions by the groups of Uemura, Selander, Shi, and Guo showed that *O*-acyl oximes derived from strained cyclic ketones could be engaged under transition-metal catalysis with Ir, Fe, Cu, or Ni.[37] At elevated temperatures, these precursors generated iminyl radicals that underwent β-scission and ring opening, providing the first catalytic entry into this reactivity. While these studies established feasibility under catalysis, their scope remained largely restricted to strained frameworks. The decisive breakthrough was achieved using visible-light photoredox catalysis. In 2018, Xiao *et al*. reported the first reductive SET protocol using an iridium photocatalyst,[38] soon followed by the group of Yu with a related system.[39] In this context, *O*-(*p*-CF$_3$-benzoyl) oximes proved particularly effective: the electron-withdrawing CF$_3$ group lowers the reduction potential and stabilizes the leaving group, aligning these precursors with the reducing power of photocatalysts such as *fac*-Ir(ppy)$_3$. By contrast, *O*-aryl oxime ethers, with higher reduction potentials, required strongly electron-deficient aryl groups (*e.g.*, nitro) to participate.[33] This evolution is summarized in Scheme 2, panel B.

Taken together, these advances established practical entry points into iminyl radicals from oxime precursors. The next question is what becomes of the resulting alkyl radicals-type **B** after β-scission. Their divergent trajectories—whether channelled into reductive or oxidative SET manifolds—determine the scope of skeletal editing. Scheme 2 (panel D) illustrates these pathways. SET-reductive manifolds: a prototypical transformation is the Giese-type addition. Radical **B** adds to an electron-deficient alkene to give radical **C**, which is subsequently oxidized by the catalyst to close the cycle. The resulting carbocation generally undergoes base-mediated deprotonation (intermolecular Heck-like) or radical–polar crossover (RPC) when trapped by a nucleophile. Alternatively, **B** can be trapped directly by SOMOphiles to forge C(sp^3)–X bonds (X = C, O, S, Se, Te, N$_3$, B, N…). In addition, it can be oxidized to a carbocation that is intercepted by ROH (ethers) or oxidized by DMSO (ketones). SET-oxidative manifolds: here, polarity is inverted. The nucleophilic δ-cyano radical **B** reacts with polarized SOMOphiles X–Y (Xδ$^+$) *via* SH$_2$/group transfer, generating the functionalized product together with Y$^\bullet$. In oxidative cycles, Y$^\bullet$ is reduced exergonically (turnover), enabling deconstructive fluorination, chlorination, azidation and related variants.

Take-home message. Cyclobutyl iminyl radicals fragment rapidly (low barrier plus strain release), whereas cyclopentyl and cyclohexyl systems require additional bias (*e.g.*, α-aryl or *gem*-dimethyl substitution, stronger oxidation, or designs that stabilize **B**). Practically, *O*-(*p*-CF$_3$-benzoyl) oximes match well with reductive manifolds, whereas α-*N*-oxycarboxylic oximes suit oxidative ones. Scheme 2 integrates these design rules.

3.1.1. Reductive approaches for deconstruction of unstrained cyclic oximes. Reductive approaches to unstrained oximes can be broadly classified into copper-mediated systems, photoredox-based manifolds, and multicomponent radical–polar crossover strategies, all of which share a strong dependence on substituent-driven stabilization.

Transition-metal reductive catalysis. Extending reductive SET chemistry to unstrained oximes is inherently difficult because the β-scission of iminyl radicals is slower and less exergonic than in strained systems, making them vulnerable to competing oxidation by copper. This limitation became evident in 2017, when Zhao and Shi attempted a Giese-type C(sp^3)–C bond formation under Cu(OTf)$_2$ at 100 °C.[37c] The reaction failed, likely because the iminyl radical fragmented too slowly, allowing copper to intercept the intermediate before productive alkyl radical addition. In contrast, cyclobutyl oximes undergo a rapid, strain-driven fragmentation, which explains why similar strategies succeed in strained substrates. In 2021, Zhao and Shi turned this drawback into an advantage.[40] By deliberately exploiting copper-mediated oxidation of the alkyl radical, they accessed carbocation intermediates that enabled divergent pathways, including β-H elimination to alkenes, C–C coupling with alkynyl sulfones, and RPC to ethers and ketones. Remarkably, they employed 2-phenylcyclopentan-1-one *O*-benzoyl oxime, where the α-aryl substituent lowers the barrier for β-scission, allowing efficient fragmentation of an otherwise less-strained system. This strategy could also apply to the late-stage functionalization of a number of complex functional molecules, such as estrone (see Scheme 3, part 1A). This observation was consistent with earlier DFT predictions.[19] In parallel, Shi, Fu, and co-workers demonstrated in 2019 that careful control of the copper environment could stabilize radical pathways (Scheme 3, part 1B).[41] Using Cu(OTf)$_2$ with 1,10-phenanthroline at 80 °C, they observed that Cu(I) could trap the alkyl radical directly to form C(sp^3)–N bonds with anilines or imines. Although the scope of unstrained oximes was narrow, this work underscored the decisive influence of the ligand sphere on the balance between radical and cationic reactivity.

Iridium photoredox reductive catalysis. Early contributions by Jiao, Shi *et al*. demonstrated that cycloketoxime esters could undergo photoinduced deconstruction/oxidation, firmly placing these transformations within the broader concept of

Open Access Article. Published on 16 June 2026. Downloaded on 6/19/2026 2:50:40 PM.
This article is licensed under a Creative Commons Attribution 3.0 Unported Licence.

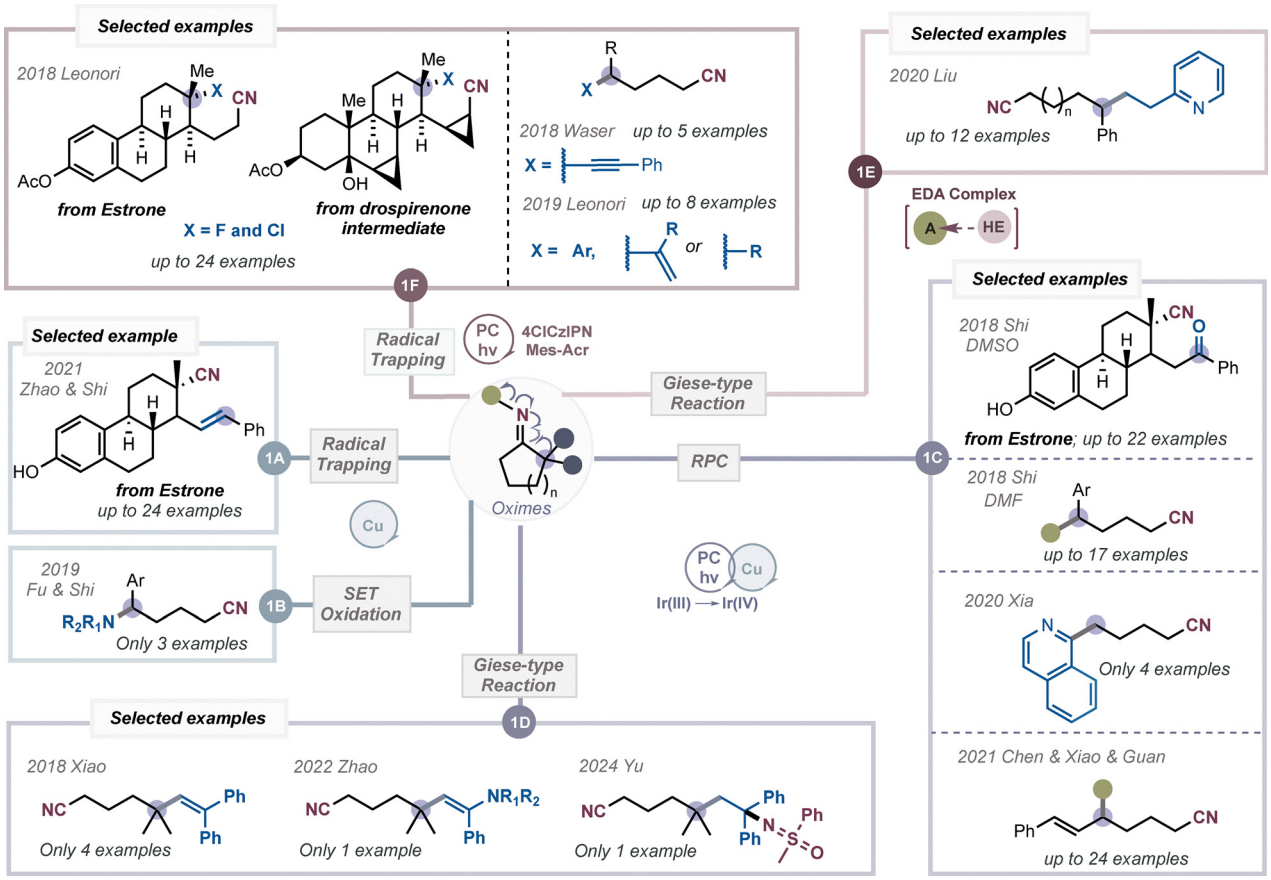

Scheme 3 Reactivity of **alkyl radical F** generated *via* iminyl-mediated ring opening of unstrained cyclic oximes. Reductive manifolds (see Section 3.1.1) proceed *via* SET activation to form iminyl radicals that undergo β-scission. The resulting **alkyl radicals F** (see Scheme 2) evolve through Cu-mediated trapping (**1A**) or SET oxidation pathways (**1B**), Ir/Cu-mediated Radical–Polar Crossover (RPC) (**1C**), Giese-type additions (**1D**), and transition-metal-free activation (**1E**). Oxidative manifolds (Section 3.1.2) generate radicals *via* polarity-inverted SET, enabling direct trapping by electrophiles (**1F**).

deconstructive functionalization of unstrained rings.[42] Representative examples included late-stage modification of complex molecules such as estrone (see Scheme 3, part 1C). The solvent played a decisive role in determining the outcome. In DMSO, acting as a terminal oxidant, the carbocation generated after RPC was further oxidized to yield ketones. In contrast, in DMF, recombination with the oxime-derived leaving group led instead to the formation of esters.[43] However, these studies also revealed that the deconstruction/functionalization process was not generally applicable. Although five-, six-, seven-, and even eight-membered rings could be opened, successful reactions consistently required an aryl substituent at the α-position of the iminyl radical to lower the barrier for fragmentation. This trend mirrored the behaviorpreviously established both computationally and experimentally.[18] Accordingly, the scope in these early photoredox studies was largely restricted to α-aryl-substituted systems (electron-neutral, -rich, and -deficient arenes tolerated).

Moving away from RPC-type manifolds, Xiao and co-workers introduced Giese-type couplings (see Scheme 3, part 1D),[38] but the reactivity window was restricted: only four examples were described, derived from camphor, cyclopentanone, and cyclohexanone oximes, and all required α-substitution by methyl, geminal dimethyl, or phenyl groups. Later, this strategy was extended to electron-deficient enamides,[44] though only one five-membered oxime bearing a geminal dimethyl group succeeded, again underlining the central role of substituent-driven stabilization in promoting β-scission. In a complementary direction, in 2020 Xia and co-workers developed Minisci-type reactions with heteroarenes (see Scheme 3, part 1C),[45] affording four examples of α-alkylated nitrogen heterocycles. However, the need for specific substitution patterns prevented broader applicability. Building on this platform, in 2024 Yu merged Giese-type reaction followed by RPC strategies to design multicomponent couplings, exemplified by the cyanoalkylsulfoximidation of alkenes (see Scheme 3, part 1D). Mechanistically, this transformation proceeds *via* a Giese-type radical addition followed by a radical–polar crossover step. Despite its synthetic appeal, the scope with unstrained oximes remains limited, with only one example reported requiring a geminal dimethyl group at the α-position to proceed efficiently.[46]

Transition metal-free photoredox reductive catalysis. In parallel to transition-metal and iridium-based photoredox approaches, metal-free strategies have been developed to improve sustainability and broaden applicability. Yu and co-

 This journal is © The Royal Society of Chemistry 2026

Open Access Article. Published on 16 June 2026. Downloaded on 6/19/2026 2:50:40 PM. This article is licensed under a Creative Commons Attribution 3.0 Unported Licence.

workers demonstrated that eosin Y, an organic dye with a suitable reduction potential, could efficiently activate cycloketoxime esters for Minisci-type cyanoalkylation of azauracils.[47] Under these conditions, strained oximes such as norcamphor-derived substrates reacted smoothly, whereas only two unstrained examples were reported, again underscoring the need for structural bias to promote fragmentation. An alternative concept was introduced using Hantzsch ester (HE) as both a photoactive reductant and hydrogen donor (see Scheme 3, part 1E). Upon visible-light excitation, HE becomes a strong single-electron reductant $\left(E^{*}_{ox} \approx -2.28\ \mathrm{V}\ vs.\ \mathrm{SCE}\right)$, capable of reducing oxime esters without requiring metal catalysts.[48] Liu and co-workers applied this concept to Giese-type couplings with 2-vinylpyridine in the presence of stoichiometric HE and further extended it to allyl sulfones. In total, up to 12 examples of unstrained systems were reported, all restricted to five, six-, and seven-membered rings bearing an α-phenyl substituent.

Photoinduced copper-catalysed ring opening. A relevant contribution in this field was reported by Guan, Xiao, and Chen, who described a photoinduced copper-catalysed asymmetric C–O cross-coupling between oxime esters and 1,3-dienes (see Scheme 3, part 1C).[49] Conceptually, this study represented a genuine paradigm shift compared to earlier reports. As outlined previously (Scheme 2, part D), an alkyl radical generated from oximes typically undergoes a Giese-type addition followed by SET oxidation (radical–polar crossover, RPC) to a carbocation, which is then deprotonated or trapped by a nucleophile. In contrast, these authors demonstrated that the alkyl radical could add to a 1,3-diene to form a resonance-stabilized allyl radical. Owing to its stabilization, this intermediate resisted oxidation and instead associated with Cu(II) together with the oxime-derived carboxylate anion to give a π-allyl Cu(III) complex, from which enantioselective C(sp^3)–O bond formation occurred. The elegance of the design lay in exploiting a known principle from benzyl radicals—namely, that resonance stabilization makes unstrained oximes reactive—yet here it was used to unlock asymmetric C–O coupling. Still, this breakthrough was only demonstrated with cyclobutanone oximes. When extending the concept to cyclopentanone oximes, the limitations became clear. Only 2-styrenyl-substituted oximes proved viable, and the reaction no longer operated as a multicomponent process involving diene trapping. Instead, SET reduction of the oxime ester directly produced an allyl radical upon ring opening, whose stabilization allowed the same copper-mediated C–O coupling with the carboxylate leaving group, now bypassing the Giese step entirely. In practice, this turned the process into an atom-economic asymmetric fragmentation/rearrangement, with the 2-styrenyl substituent playing the same role that α-aryl groups in earlier reports, though through a mechanistically distinct pathway. Up to 24 examples were reported, highlighting both the originality of the concept and its structural constraints. Notably, a biologically relevant febuxostat-derived 1,3-diene also coupled efficiently with 2-styrenyl-substituted oximes to afford the desired product.

In summary, reductive approaches have provided valuable mechanistic insights and some notable advances, particularly in enantioselective copper catalysis. However, their generality remains limited: productive fragmentation still relies on deliberately introduced structural bias (*e.g.*, α-substitution or geminal stabilisation), and extension to complex scaffolds has been rare. While isolated cases of late-stage deconstruction/functionalization exist, they have not yet established a broadly applicable platform. These constraints highlight that further innovations are needed if reductive manifolds are to achieve the same level of versatility already observed in oxidative strategies.

3.1.2. Oxidative approaches for deconstruction of unstrained cyclic oximes. Oxidative SET activation of oxime carboxylates was first introduced in 2018 by some of the present authors[19] as a complementary entry to reductive pathways (see Scheme 3, part 1F). This polarity inversion enabled the generation of alkyl radicals *via* β-scission, which could then be trapped by electrophilic partners to achieve deconstructive fluorination, chlorination, and azidation. Unlike earlier methods, this strategy was not limited to strained substrates but extended effectively to unstrained five- to seven-membered rings. It also proved suitable for late-stage functionalization of bioactive molecules such as androsterone, prasterone, estrone, drospirenone, camphor, and isosteviol---demonstrated across 24 examples. These results underscore the utility of oxidative SET in accessing fluorinated, chlorinated, and azidated analogs of pharmacologically relevant scaffolds, offering clear advantages for drug discovery.

Waser and co-workers subsequently exploited the same principle with ethynylbenziodoxolones (EBX) as electrophilic SOMOphiles, achieving visible-light-mediated alkynylation (see Scheme 3, part 1F).[50] The incorporation of alkynes is particularly appealing in medicinal chemistry, since these motifs serve both as pharmacophores and as handles for bioorthogonal click-type derivatizations. However, the method was applied to only five examples of unstrained five-membered rings.

Zhou *et al.* later demonstrated that oxime-derived alkyl radicals could also participate in oxidative Giese-type additions to trifluoromethyl alkenes.[51] After addition, the resulting α-CF_3 radical underwent SET reduction to a carbanion, followed by β-fluoride elimination to give cyano-substituted *gem*-difluoroalkenes. Such fluorinated motifs are highly valued in medicinal chemistry because they can enhance the metabolic stability, lipophilicity, and binding affinity of drug candidates. However, this approach was only applied to six examples, all limited to five-membered rings. In parallel, Yang *et al*. reported a photocatalytic phosphoranyl radical-mediated strategy for the direct N–O cleavage of strained cycloketone oximes *via* a polar/SET crossover.[52] Unlike previous methods relying on aryl or acyl oximes, this approach directly activated the oxime itself, broadening functional group tolerance. However, its application to unstrained cyclic oximes has not yet been demonstrated.

Despite these advances, a persistent limitation of both reductive and oxidative SET manifolds is that alkyl radicals formed after oxime scission often lack direct handles for cross-

Open Access Article. Published on 16 June 2026. Downloaded on 6/19/2026 2:50:40 PM.
This article is licensed under a Creative Commons Attribution 3.0 Unported Licence.

coupling, restricting the diversity of accessible transformations. To overcome this, Leonori and co-workers merged photoredox activation with nickel catalysis,[53] enabling direct arylation, vinylation, and alkylation of nitrile frameworks (see Scheme 3, part 1F). This dual catalytic design represented a major step forward. By orchestrating two interconnected cycles, oxime-derived radicals could be diverted into C–C bond-forming cross-couplings that expand the scope of deconstructive functionalization far beyond classical radical reactivity. The approach was applied to eight examples, limited to five- and six-membered rings.

Future perspective. Despite rapid progress, the deconstruction of ketone *via* oxime radical chemistry still faces important challenges. Enantioselective transformations remain rare: beyond the asymmetric C–O cross-coupling of Guan, Xiao, and Chen,[49] general methods are lacking. The authors suggested that expanding stereocontrol through γ-chiral oximes[54] or by harnessing biocatalysis[36] represents promising future directions. A key bottleneck is the limited reactivity of unprotected oximes. While activating groups such as carbonates, esters, ethers or α-imino-oxy acids efficiently promote N–O bond cleavage, they increase synthetic cost and complexity. Direct use of free oximes as iminyl precursors is attractive, but side reactions—including *N*-oxyl radical formation, acid-promoted rearrangements, and hydrolysis—often suppress the desired reactivity. These issues explain why stoichiometric additives such as PPh_3 are still commonly required. Looking ahead, innovative catalytic paradigms may overcome these limitations. Dual photoredox/Ti dehydroxylation,[29a,b] which is currently restricted to strained substrates, could be extended to unstrained scaffolds. The authors further anticipate that the use of chiral Ti complexes could also provide new avenues for stereocontrol. Alternatives such as *N*-iminopyridinium salts[29c] are already broadening the accessible chemical space, and EDA complexes hold particular promise for improving reactivity in challenging systems—for instance, by exploiting intramolecular EDA activation in combination with chiral donor catalysts to drive stereoselective radical reactions. Ultimately, the promise of oxime radical chemistry extends beyond achieving stereocontrol, offering powerful opportunities for late-stage functionalization that enable the redesign of bioactive cores and the exploration of novel chemical space.

3.2. Aminium radicals: deconstructive functionalization to spirocycles

As we have seen throughout this tutorial, the activation of C–C bonds in unstrained cyclic ketones represents a demanding challenge, and successful approaches consistently rely on the introduction of a thermodynamic driving force. Different strategies illustrate this principle. Alkoxy radicals derived from alcohols undergo β-scission to give ring-opening products; oxime derivatization offers an indirect route to C–C bond cleavage, proceeding through an iminyl radical precursor rather than direct activation of the ketone; and LMCT photooxidation, in which a ketone forms an *in situ* cyanohydrin under Lewis acid activation before photoexcitation, enables

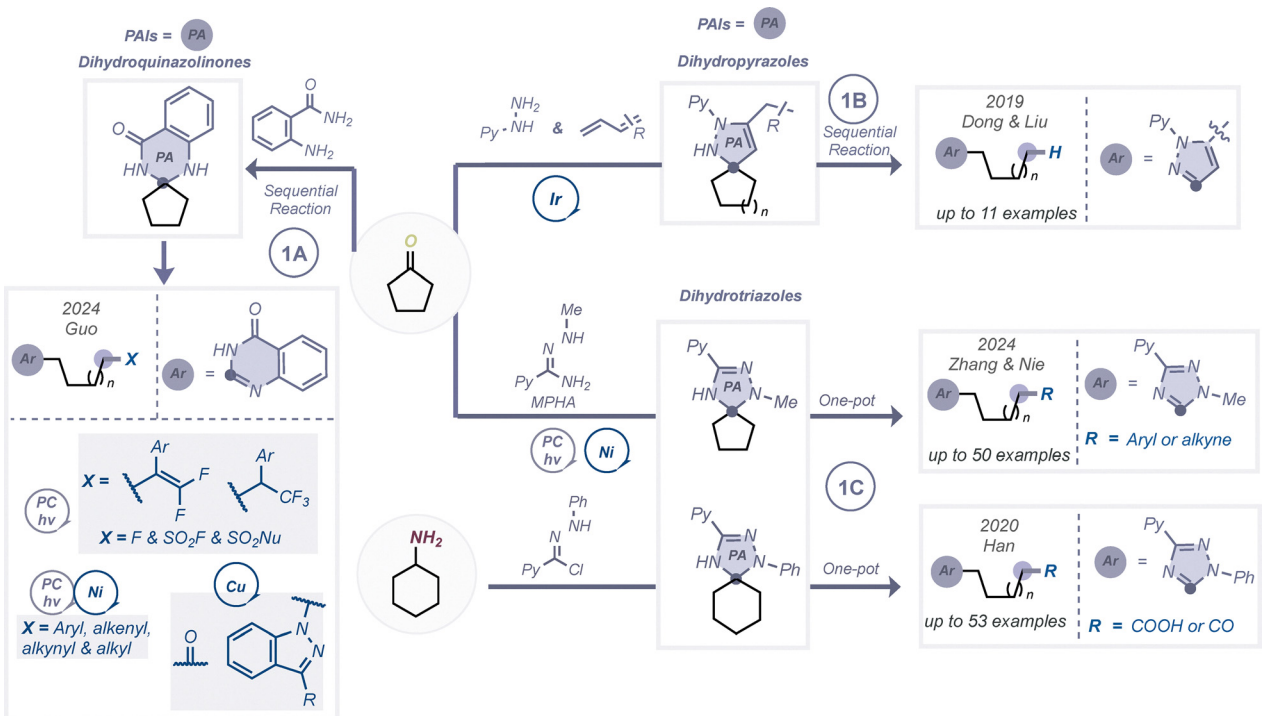

Scheme 4 Aromatization-driven C–C bond cleavage *via* pre-aromatic intermediates. (**1A**) Dihydroquinazolinone PAIs from cyclic ketones. (1B) Dihydropyrazole PAIs formed *via* hydrazone/[3+2] cycloaddition, enabling deconstructive pyrazole formation. (**1C**) Dihydrotriazole PAIs generated using MPHA, enabling mild SET-oxidative or dual catalytic deconstruction and functionalization.

Open Access Article. Published on 16 June 2026. Downloaded on 6/19/2026 2:50:40 PM. This article is licensed under a Creative Commons Attribution 3.0 Unported Licence.

homolysis of the C–O bond to release an *O*-centered radical.[55] Despite their mechanistic diversity, all these cases share the same underlying feature: the reactivity is redirected along a more favourable energetic landscape. A complementary way to establish this bias is through the gain of aromatic stabilization, a powerful thermodynamic force both in enzymatic and synthetic contexts. In steroid biosynthesis, for example, aromatase converts testosterone into estradiol through a multi-step oxidative sequence, that includes C–C cleavage.[56] The stabilizing effect of aromatization has also been recognized in transition-metal-mediated C–C activation since the 1970s,[57] although only sporadically explored in subsequent decades.[58] Building directly on this concept, pre-aromatic intermediates (PAIs) have recently emerged as a general solution, converting difficult C–C scission into an aromatization-driven process. Three main families have been established—dihydroquinazolinones, dihydropyrazoles, and dihydrotriazoles—each functioning as radical precursors that enable productive deconstruction and functionalization. (See Scheme 4).

Dihydroquinazolinone PAIs (see Scheme 4, 1A)[59] arise from 2-aminobenzamide/ketone condensations and have enabled a series of deconstructive transformations, although their use in non-strained cyclic systems is still limited.[60] Building on this, Guo developed spiro-dihydroquinazolinones from cycloalkanones, which undergo: (i) photoredox/nickel cross-coupling with organic halides;[61] (ii) coupling with α-CF_3 alkenes;[62] (iii) deconstructive fluorination with NSFI;[63] (iv) copper/ROOR-mediated amination *via* HAT/β-scission and $R_1R_2NCu(II)$ capture;[64] and (v) fluorosulfonylation using DABSO/NSFI.[65] While these reactions highlight the synthetic potential of the platform, the condensation step often proceeds with only moderate efficiency due to the low nucleophilicity of the amide moiety, frequently requiring purification before C–C cleavage.

Dihydropyrazole PAIs (see Scheme 4, 1B), first reported by Dong and co-workers, constitute another important advance.[1d] In this system, an iridium/phosphine catalyst promotes a three-component sequence of ketone, hydrazine, and a 1,3-diene: hydrazone formation is followed by [3+2] cycloaddition with the diene to generate a dihydropyrazole, which then fragments to deliver a pyrazole (a key pharmacophore in medicinal chemistry) together with a reactive alkyl radical. Importantly, cyclic ketones can be directly engaged, enabling a redox-neutral deconstructive synthesis of pyrazoles. The bond scission occurs preferentially at substituted, benzylic, or α-to-heteroatom positions, allowing access to structurally diverse pyrazoles across multiple cyclic substrates. However, the requirement for excess 1,3-diene, high temperature (160 °C), and iridium-catalysed olefin migration reduces the substrate scope, highlighting the need for next-generation activating reagents that can promote aromatization-driven cleavage under milder conditions.

Dihydrotriazoles PAIs (see Scheme 4, 1C), have emerged as a promising alternative to to the previously mentioned methodologies. *N*′-methylpicolino-hydrazonamide (MPHA) was developed to access such PAIs under mild conditions. MPHA meets key needs: it is inexpensive, reacts rapidly and cleanly with ketones without purification, and enables C–C cleavage of diverse substrates under mild conditions. It has served as a driving force in the deconstructive oxygenation of cycloalkanamines.[66] Since cyclic amines are ubiquitous in drugs and natural products,[67] the Han group showcased a one-pot protocol for *in situ* formation of 3,4-dihydro-1,2,4-triazoles from cycloalkanamines and hydrazonyl chlorides, followed by auto-oxidative annulation using air as terminal oxidant. Further oxidation by air generates aminyl radicals that promote C–C bond cleavage, enabling the regioselective deconstructive oxygenation of a wide range of substrates—including mono-, fused-, and bridged-cyclic amines, as well as alkaloids, peptides, and steroids—in up to 53 reported examples.

In ketone chemistry, the enhanced nucleophilicity of MPHA compared to amides facilitates efficient condensation, and Dong and co-workers demonstrated oxidative cleavage of dihydrotriazoles to generate carbon-centred radicals. These intermediates were diversified into alkenes,[68] hydrogenated or deuterated products,[69] thioethers,[70] and halogenated derivatives.[71] Nevertheless, the application of MPHA-based dihydrotriazoles to the ring-opening of unstrained cyclic ketones has not yet been carried out.

More broadly, PAI-based approaches with ketones still face practical limitations, as intermediates often require pre-isolation or elevated temperatures.[72] To overcome these drawbacks, Zhang and co-workers applied MPHA-derived PAIs strategically, whose clean and rapid formation eliminates the need for purification, and combined them with a dual nickel/photoredox system that operates under mild conditions.[73] This design enabled the cross-coupling of unstrained cyclic ketones with aryl bromides, including late-stage functionalization of derivatives of DL-proline, naproxen, febuxostat, dopamine, and gemfibrozil. The method was further extended to alkynylation, capitalizing on the synthetic versatility of alkynes, which are widely represented in natural products, pharmaceuticals, and functional materials. Even ketone derivatives of naproxen and ketoprofen underwent smooth functionalization, underscoring the broad compatibility of this approach with drug-like scaffolds. Overall, the combination of MPHA activation with dual catalysis provides one-pot efficiency, broad functional group tolerance, and applicability to complex molecules, thereby addressing the major limitations of earlier PAI chemistry.

3.3. Alkoxy radicals from unstrained cyclic alcohols: activation strategies and reactivity manifolds

As discussed in Sections 1 and 2, alkoxy radicals ($RO^{\bullet}$) constitute a reliable gateway for C–C bond cleavage in unstrained cyclic frameworks through fast β-scission. Although this reactivity has long been recognised, the direct generation of $RO^{\bullet}$ from native alcohols without prefunctionalisation has historically remained a major challenge, owing to the high strength of the O–H bond and competing reaction pathways. What has changed in recent years, and now reshapes the landscape of skeletal editing, is the emergence of complementary activation strategies that effectively overcome this barrier. As documented in recent reviews,[15a,b,16,74] alcohol activation has shifted from a high-energy bottleneck to a solvable design problem, whether

Open Access Article. Published on 16 June 2026. Downloaded on 6/19/2026 2:50:40 PM. This article is licensed under a Creative Commons Attribution 3.0 Unported Licence.

by matching bond energetics through PCET (bond dissociation free energy, BDFE, logic),[74b] leveraging metal coordination *via* LMCT, or exploiting radical frustration (RPF). To organise this chemistry, we adopt a two-step framework depicted in Scheme 5. Step 1 focuses on the direct generation of the **alkoxy radical E** from non-strained cyclic alcohols. Three conceptually distinct platforms are highlighted: PCET-based processes, LMCT-based activation, and frustrated radical pair (FRP) manifolds (top view of Scheme 5). Although these strategies differ in mechanism, they converge on the same key intermediate and are governed by different controlling factors, which are indicated schematically in Scheme 5 and discussed in detail in the corresponding sections. Step 2 addresses the fate of the **alkyl radical F** formed after β-scission (bottom view of Scheme 5), where divergent reactivity modes become accessible, including radical trapping, Giese-type additions, radical–polar crossover processes, and dual catalytic cross-couplings (among others).

The following sections are therefore organised to provide practical guidelines for selecting among these activation strategies. In each subsection, we first outline the key design principles required to generate an effective **alkoxy radical E** (Scheme 5, Step 1), and then evaluate the downstream reactivity of the resulting **alkyl radical F** after ring opening, which governs the final functionalisation outcome (Scheme 5, Step 2). Section 3.3.1 examines PCET-based processes, where reactivity is mainly dictated by thermodynamic parameters and outer-sphere interactions. Section 3.3.2 discusses how dual catalytic manifolds, combining PCET with transition-metal catalysis, expand the accessible reactivity space. Section 3.3.3 presents LMCT-based processes, highlighting the role of inner-sphere metal–substrate coordination and metal-dependent redox windows. Finally, FRP-based strategies are introduced as an emerging and mechanistically distinct approach in Section 3.3.4, operating through in-cage radical pairs. While the activation modes differ, all these strategies converge on closely related **alkyl radical F** intermediates. Accordingly, Scheme 6 summarises selected examples of Step 2 reactivity, providing a unified map of **alkyl radical F**unctionalisation outcomes accessed *via* PCET-, LMCT-, or FRP-based approaches. In this context, the emphasis is placed on the synthetic milestone achieved, allowing direct comparison of how a given transformation can be realised through different activation paradigms. Section 3.3.5 then discusses miscellaneous or hybrid cases that do not fit cleanly into these categories but further illustrate the breadth of alkoxy-radical-mediated deconstruction.

Across PCET-, LMCT-, and FRP-based platforms, alkoxy radicals are generally generated through oxidative activation of the parent alcohol, such that formation of the downstream **alkyl radical F** originates from an overall SET-oxidative manifold.

3.3.1. PCET-based processes. PCET has emerged as a central framework for the activation of strong O–H bonds. Its impact extends far beyond synthetic chemistry, underpinning key transformations in biological energy transduction such as photosynthesis, respiration, and enzymatic radical generation.[75] The conceptual strength of PCET lies in coupling proton (H^+) and electron (e^-) motion, thereby enabling reactivity that neither isolated proton transfer (PT) nor electron transfer (ET) could accomplish. Mechanistically, three steps can be defined: (i) PT followed by ET, (ii) ET followed by PT, or (iii) a concerted proton–electron transfer (CPET), in which both elements move in a single kinetic step. The latter is generally favoured because it avoids unstable ionic intermediates, and Evans, Savéant and co-workers emphasized this distinction with the explicit term CPET as previously described.[76] From a thermodynamic perspective, the driving force of PCET can be described using a small set of interrelated parameters (see top view in Scheme 5, 1st step, part A): the acidity constants (pK_a) of the oxidized and reduced states, the reduction potentials (E°) of the protonated and deprotonated forms, and the bond dissociation free energy (BDFE). Unlike the purely enthalpic bond dissociation energy (BDE), the BDFE accounts for entropic contributions, which are especially relevant in transition-metal systems. Building on this, Mayer and Warren introduced the concept of the effective BDFE ($BDFE_{eff}$), which quantifies the combined ability of an oxidant and a base to remove a hydrogen atom from an X–H bond.[77] This framework provides a practical design principle: if $BDFE_{eff} \geq BDFE(X–H)$, bond cleavage by PCET is thermodynamically accessible. Importantly, this dual tuning through E° and pK_a opens an energetic window not available to classical hydrogen-atom transfer (HAT) reagents.[78]

In practice, three distinct PCET manifolds can be distinguished, as outlined (see top view in Scheme 5, part A): unidirectional PCET (**A1**), multisite PCET (MS-PCET) (**A2**), and SET–MS PCET involving a redox handle (**A3**). In the unidirectional pathway **A1**, proton and electron transfers proceed in a concerted directional manner, often through electron donor–acceptor (EDA) complexes, which directly couple bond activation with radical capture. MS-PCET **A2**, by contrast, relies on independent oxidant and base partners. This separation allows the two transfers to be spatially and energetically decoupled, which in turn broadens the accessible range of effective BDFEs. As a result, this strategy enables the activation of otherwise inert O–H bonds. A third scenario, SET–MS PCET with a redox handle (**A3**), introduces an adjacent substituent—typically an aromatic moiety—that is first oxidized and then promotes intramolecular proton transfer, offering strong preorganization and efficient bond cleavage. Together, these manifolds illustrate the versatility of PCET logic: depending on the design, it can favour simplicity and integration (unidirectional), broad thermodynamic reach (MS-PCET), or structural preorganization (SET–MS PCET with a handle). In the following sections, we will focus on specific applications, examining how PCET activation of alcohols is harnessed in different reactivity modes.

Radical Trapping (see Scheme 6, part 1A to follow the section): The first catalytic PCET strategy for direct alkoxy radical generation was reported in 2016 by Knowles and co-workers (see Scheme 6, 1A left), who showed that tertiary cycloalkanols bearing electron-rich aryl substituents undergo SET–MS PCET with a redox handle (see Scheme 5, step 1, A).[79] The resulting alkyl radical is then trapped *via* a hydrogen-atom

 This journal is © The Royal Society of Chemistry 2026

Open Access Article. Published on 16 June 2026. Downloaded on 6/19/2026 2:50:40 PM.
This article is licensed under a Creative Commons Attribution 3.0 Unported Licence.

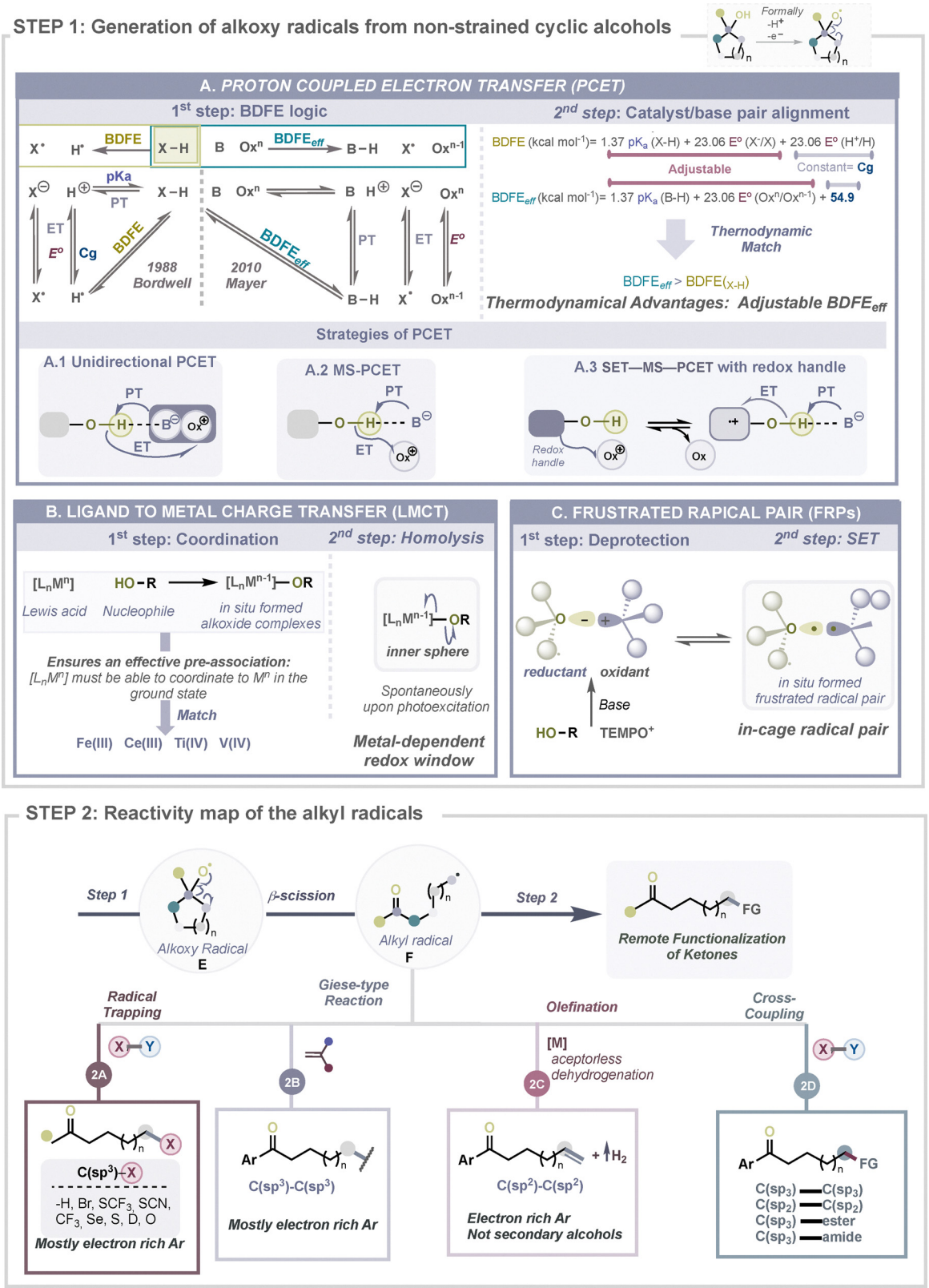

Scheme 5 Activation of unstrained cyclic alcohols *via* alkoxy radicals. Step 1: direct generation of **alkoxy radical E** from non-strained cyclic alcohols through three complementary activation strategies: PCET-based processes (unidirectional PCET, multisite (MS) PCET, and SET-assisted MS-PCET), LMCT-based activation *via* metal coordination, and frustrated radical pair (FRP) manifolds. The key thermodynamic and mechanistic control elements governing O–H bond cleavage are indicated. Step 2: reactivity map of the **alkyl radical F** formed after β-scission, which is common to all alkoxy-radical generation modes and gives access to radical trapping, Giese-type additions, radical–polar crossover pathways, and dual catalytic cross-couplings.

Open Access Article. Published on 16 June 2026. Downloaded on 6/19/2026 2:50:40 PM.
This article is licensed under a Creative Commons Attribution 3.0 Unported Licence.

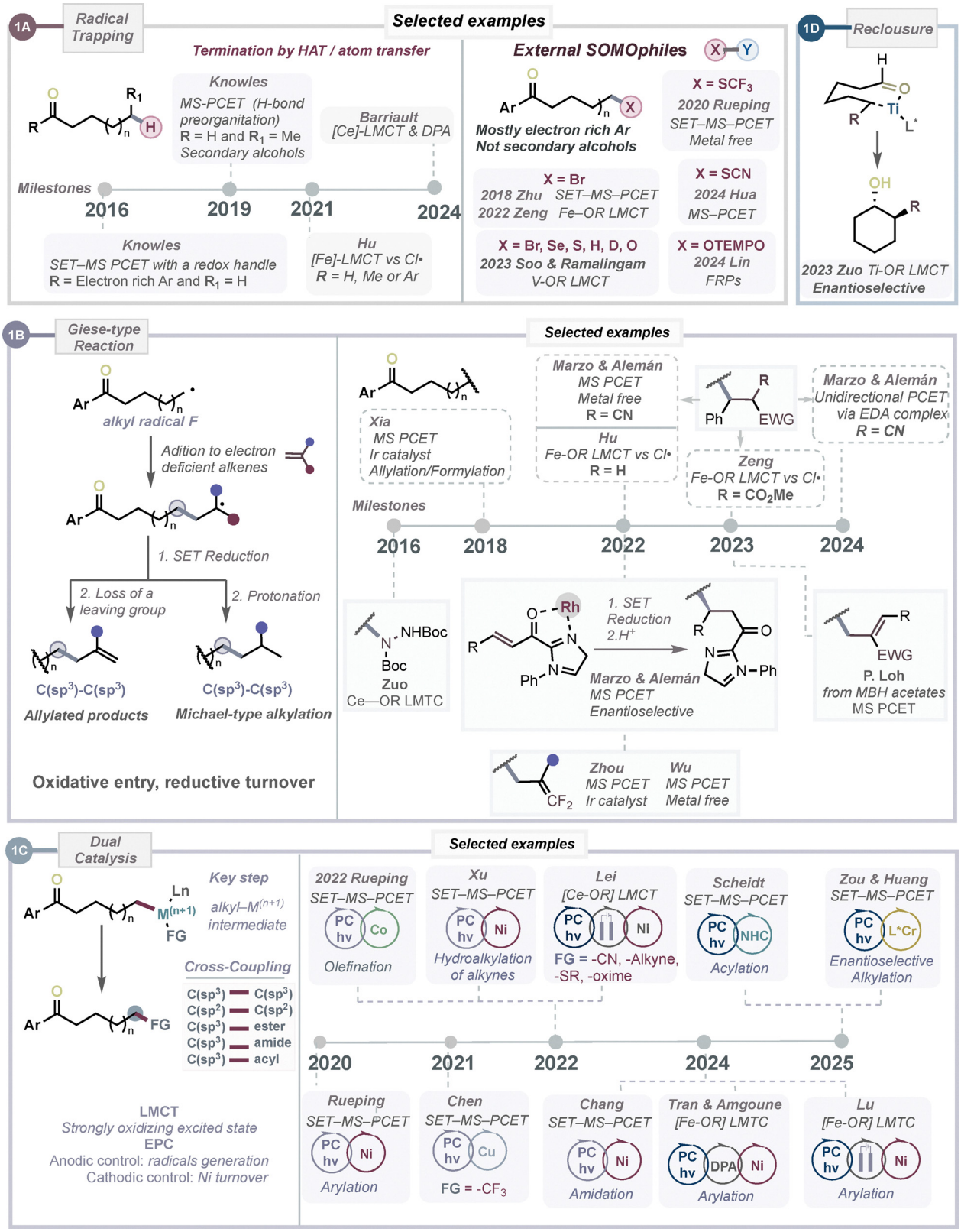

Scheme 6 Reactivity manifolds of alkyl radicals formed from unstrained cyclic alcohols after β-scission. (1A) Radical trapping, *via* hydrogen- or atom-transfer processes, typically delivers reduced or heteroatom-substituted products and is favoured for less-stabilised radicals. (1B) Giese-type addition involves radical addition to electron-deficient alkenes, followed by reduction and protonation, enabling C(sp^3)–C(sp^3) bond formation across PCET, LMCT, and metal-free platforms. (1C) Dual catalysis embeds **alkyl radical F** into a metal-centred catalytic cycle, either through formation of alkyl–metal intermediates or related radical–metal association events (M = Ni, Co, Cu, Cr), enabling cross-coupling, desaturation, or asymmetric functionalisation. (1D) Reclosure (Ti-LMCT): β-scission followed by recombination (enantioselective).

 This journal is © The Royal Society of Chemistry 2026

Open Access Article. Published on 16 June 2026. Downloaded on 6/19/2026 2:50:40 PM. This article is licensed under a Creative Commons Attribution 3.0 Unported Licence.

transfer (HAT) process, defining this transformation as a radical trapping manifold. In this redox-relay system, photoexcited [Ir(dF(CF$_3$)ppy)$_2$(5,5′-d(CF$_3$)bpy)] (E^* ≈ +1.30 V *vs.* Fc/Fc$^+$) oxidizes the arene (E° ≈ +1.18–1.27 V *vs.* Fc/Fc$^+$), forming Ar$^{\bullet+}$, which engages in intramolecular PCET with 2,4,6,-collidine (pK_a ≈ 15 in MeCN) to cleave the O–H bond. The effective BDFE (103–105 kcal mol^{-1}) matches the strength of aliphatic O–H bonds, ensuring thermodynamic feasibility. Importantly, mechanistic probes indicated that stepwise PT/ET would be too endergonic (ΔG° ≈ +34 kcal mol^{-1}) to compete with charge recombination (ΔG° ≈ −53 kcal mol^{-1}). However, concerted PCET is slightly exergonic (ΔG° ≈ −1 kcal mol^{-1}) and operative even when up to four methylenes separate the arene from the alcohol, supporting a concerted pathway. This study was a landmark demonstration of contrathermodynamic skeletal editing: β-scission drives conversion to linear ketones that are less stable than the cyclic precursors, with downstream HAT and charge recombination enforcing directionality. The approach proved compatible with natural product derivatives, such as a hecogenin analogue, and allowed distal functionalization with halogen donors (F, Cl, Br) as alternatives to thiols, furnishing halogenated ketones. The key limitation was the need for a proximal electron-rich aryl substituent to mediate O–H activation *via* SET–MS PCET, restricting scope largely to tertiary cyclic alcohols. In 2019, Knowles and co-workers extended the scope of catalytic PCET beyond tertiary substrates to include secondary cyclic alcohols (see the milestone in Scheme 6, 1A).[80] This advance relied on tetrabutylphosphonium dimethyl phosphate ($PBu_4^+(MeO)_2PO^-$) as the base, which forms a strong hydrogen-bonded complex with the alcohol and enables a true MS-PCET manifold (Scheme 5, Step 1, A). In this case, photoexcited Ir(III)* (E^* ≈ +1.65 V *vs.* Fc/Fc$^+$) and the phosphate base (pK_a ≈ 12 in MeCN) act cooperatively to cleave the O–H bond, delivering an effective BDFE of 103–106 kcal mol^{-1}, closely matching the intrinsic O–H bond strength of secondary alcohols such as cyclohexanol (∼105 kcal mol^{-1}). As in the earlier work, β-scission is followed by radical trapping *via* HAT, with subsequent charge recombination providing kinetic control. This strategy enabled skeletal editing of complex polycyclic frameworks, including cholesterol and betulin derivatives.

Beyond these seminal examples, radical trapping constitutes a general and modular outlet for PCET-generated alkoxy radicals, in which the **alkyl radical F** formed after β-scission is intercepted by an external SOMOphile through HAT or atom-transfer processes (see Scheme 6, 2A left and right, respectively). In this sense, in 2018 Zhuo *et al.* reported that tertiary cycloalkanols bearing aryl substituents undergo efficient bromination in the presence of [Ir(ppy)(dtbbpy)]PF$_6$ and hypervalent iodine reagents.[81] The alkoxyl radical is proposed to arise either by intermolecular PCET involving the Ir(IV) species and a weak base such as succinimide ($E_{1/2}$[Ir(IV)/Ir(III)] = +1.21 V *vs.* SCE; pK_a ≈ 13–15), or alternatively by *in situ* O–I bond homolysis. In both scenarios, visible light is indispensable, and β-scission delivers a distal alkyl radical that is trapped by NBS to give brominated products. Building on this strategy, in 2020 Rueping and co-workers described a trifluoromethylthiolation using Mes–Acr$^+$ (E^* ≈ +2.06 V *vs.* Fc/Fc$^+$) as photocatalyst and 2,4,6-collidine as base (pK_a ≈ 15 in MeCN), where the effective BDFE matches the O–H bond strength of the alcohol substrate.[82] In this case, the **alkyl radical F**ormed after β-scission is intercepted by PhthSCF$_3$, generating the SCF$_3$-substituted product while the phthalimidyl radical is reduced and protonated to close the cycle. Hua and co-workers reported in 2024 that tertiary cycloalkanols undergo β-scission/thiocyanation under photoredox conditions using *N*-thiocyanatosaccharin as the SCN source.[83] The system employs 4,6-triphenylpyrylium tetrafluoroborate (TPT, E^* ≈ +2.3 V *vs.* SCE) as photocatalyst together with Na_2CO_3 (20 mol%) under blue LED irradiation. The authors proposed a direct SET oxidation of the alcohol by TPT*, generating an alkoxyl radical. However, oxidation potentials of simple alcohols generally exceed +2.0 V *vs.* SCE, making such a process unlikely, and it would bypass the strength of the O–H bond (≈ 105 kcal mol^{-1}). In our opinion, a more consistent view is that the reaction proceeds *via* a MS-PCET pathway. In this sense, a TPT* can combine with the weak basicity of carbonate. Although Na_2CO_3 is far too weak to deprotonate an alcohol in MeCN (pK_a ≈ 40), its cooperative interaction with the strong photooxidant could provide an effective BDFE (≈115–118 kcal mol^{-1}), sufficient to cleave the O–H bond. In either case, the key intermediate is an alkoxyl radical that undergoes β-scission to give a distal radical, subsequently trapped by SCN$^\bullet$ from the thiocyanatosaccharin precursor to deliver the thiocyanated product.

Giese-type reaction (see Scheme 6, part 1B for selected examples): a prototypical transformation in this field, in which PCET-triggered β-scission is coupled to radical addition. The addition of nucleophilic **alkyl radicals F** to electron-deficient alkenes provides a robust and broadly applicable strategy for C–C bond formation. A key distinction from iminyl-derived systems lies in the redox polarity of the catalytic cycle (see Scheme 2 *vs.* Scheme 6). In oxime-based deconstructions, **alkyl radicals B** are typically generated *via* reductive SET, and Giese-type addition is usually followed by oxidative SET to achieve catalytic turnover. By contrast, in alkoxy-radical-mediated processes, the **alkyl radical F** is accessed through an oxidative entry manifold, such that productive turnover after Giese-type addition requires a subsequent reductive SET step. In this sense, in 2018, Xia *et al.* showed that PCET-triggered β-scission can be coupled to radical additions, enabling distal allylation and formylation under photoredox conditions.[84] In this work, the **alkyl radical F** generated upon ring opening adds to ethyl 2-(phenylsulfonyl)methyl)acrylate, and reduction of the resulting intermediate promotes elimination of PhSO$_2^-$, furnishing the allylated product. Building on this concept, Zhou and co-workers disclosed a defluorinative coupling of cycloalkanols with trifluoromethyl alkenes to access gem-difluoroalkenes.[85] After radical addition to the alkene, RPC provides an α-CF$_3$ carbanion that undergoes β-fluoride elimination. This sequence has also been performed under metal-free, visible-light-driven conditions by the group of Wu (see Scheme 6).[86] More recently, in 2023 Loh *et al.* extended this platform to a

Open Access Article. Published on 16 June 2026. Downloaded on 6/19/2026 2:50:40 PM. This article is licensed under a Creative Commons Attribution 3.0 Unported Licence.

formal Grob fragmentation, where Morita–Baylis–Hillman (MBH) acetates serve as radical traps to access unsaturated ketones (see Scheme 6, part 1B right).[87] In this transformation, the distal radical adds to the MBH double bond to form the corresponding alkyl radical intermediate, which undergoes SET reduction by the reduced acridinium catalyst to generate a stabilized anion. The EWG on the MBH framework is essential, as it stabilizes the carbanion and promotes β-elimination of acetate, ultimately delivering a conjugated enone product. In 2022, Marzo, Alemán, and co-workers reported a classical Giese-type addition of **alkyl radical F** to electron-deficient alkenes under metal-free photoredox conditions, using [Mes–Acr]ClO_4 as photocatalyst.[88] The resulting radical undergoes reduction and protonation to deliver remote Michael-type alkylation products (Scheme 6, part 1B). Chowdhury and co-workers subsequently disclosed a related variant leading to ketone formation.[89] Here, the distal radical is trapped by a β-silylmethylene malonate. A particularly interesting advance was reported by Marzo and Alemán in 2022, who developed an enantioselective version of this transformation (see Scheme 6, part 1B).[90] In their design, they employed similar conditions to previously described photoredox β-scission protocols, but in the presence of chiral rhodium catalysts. After scission of the β-C–C bond, the alkyl radical undergoes addition to an *N*,*O*-Rh-coordinated 2-acyl imidazole. The sterically encumbered and chiral environment of the Rh complex enforces selective addition through the less hindered face, generating a stereodefined radical intermediate. This radical is subsequently reduced by the radical anion of the photocatalyst and, after protonation, delivers the enantioenriched product, thereby closing the photocatalytic cycle. This work illustrates how the merger of PCET-driven β-scission with asymmetric catalysis enables access to enantioselective variants of Giese-type processes, expanding the synthetic reach of this platform. An elegant variation arises when the alcohol and an electron-deficient alkene form a visible-light-active EDA complex. In this sense, Marzo and Alemán group reported that, upon excitation, charge transfer within the complex triggers a unidirectional PCET: the alkene simultaneously promotes O–H bond activation and captures the resulting alkyl radical through a Giese addition.[91] This design contrasts with MS-PCET and SET–MS-PCET, as no external photocatalyst or base is required; the acceptor itself mediates both proton and electron transfer. Conceptually, this constitutes a direct coupling of activation and trapping in a single step. Practically, the simplicity of the system and its compatibility with flow setups offer clear advantages for scale-up, though the lack of independent control over redox and Brønsted parameters limits its thermodynamic flexibility compared to MS-PCET strategies.

3.3.2. Dual PCET-based processes. Radical trapping (Scheme 6, panel 1A) and Giese-type manifolds (Scheme 6, part 1C) provide efficient entry points for functionalising the **alkyl radical F** generated after β-scission. However, in both cases, reactivity remains governed by the intrinsic behaviorof freely diffusing radicals, which inherently limits chemoselectivity, substrate scope, and the range of accessible bond constructions. In radical trapping, selectivity is dictated by the nature of the SOMOphile, whereas in Giese-type processes it is controlled by polarity matching and subsequent SET events. Dual catalytic strategies overcome these intrinsic limitations by fundamentally changing the reactivity regime of F (Scheme 6, part 1C). Rather than allowing F to evolve as a free radical, it is rapidly embedded into a metal-centred catalytic cycle through formation of an **alkyl–M$^{(n+1)}$** intermediate. From this point onwards, reactivity is dictated by the elementary steps available to the metal centre, enabling transformations that are inaccessible under purely radical conditions. Although the identity of the metal varies, the deliberate generation of **alkyl–M$^{(n+1)}$** species is the defining feature of this class, providing a unified framework for cross-coupling or olefination, among others, in PCET strategies.

Radical trapping (–CF_3). In 2021, Chen and co-workers developed a dual photoredox/copper strategy for the trifluoromethylation of tertiary cycloalkanols using Togni I reagent (see Scheme 6, part 1C).[92a] The system combines [Mes–Acr–Ph]BF_4 (E^* ≈ +2.08 V *vs.* SCE), $Cu(OAc)_2$, and $n$$Bu_4P^+(OMe)_2POO^-$ as base. Mechanistic evidence supports a phosphate-assisted MS-PCET activation of the alcohol, in line with PCET manifolds previously established by Knowles. However, due to the study focused on aryl-bearing tertiary alcohols, a SET–MS PCET relay *via* aryl radical cation intermediates cannot be ruled out. Additional fluorescence and NMR studies suggested that Togni I (a hypervalent iodine(III) CF_3-transfer reagent) can interact noncovalently with the alcohol, facilitating oxidative quenching, although this effect appears secondary to the PCET step. Following generation of the **alkoxy radical E** and β-scission (see Scheme 5, Step 2), the resulting **alkyl radical F** is intercepted within the copper catalytic manifold (Scheme 6, part 1C). In this system, CF_3 incorporation does not proceed *via* free CF_3 radical transfer, but through Cu-mediated steps. Togni I serves as the CF_3 source and reacts with Cu(I) under oxidative conditions, promoting I–CF_3 bond cleavage and formation of a higher-valent Cu–CF_3 species. This step is consistent with the electrophilic nature of the reagent and its ability to engage in SET under photoredox conditions. The resulting Cu(III)–CF_3 intermediate enters the photoredox cycle, where SET with the reduced photocatalyst ($Acr^\bullet$) regenerates the ground-state catalyst and forms a Cu(II)–CF_3 species. The **alkyl radical F** is then captured by the Cu–CF_3 fragment, leading to C–CF_3 bond formation and regeneration of Cu(I), thus closing the catalytic cycle. As shown in Scheme 6 (part 1C), the key feature is interception of radical F within a metal-controlled manifold. While a discrete alkyl–Cu(III) intermediate cannot be excluded, available evidence is consistent with direct capture of the carbon-centred radical by Cu–CF_3 species. Accordingly, the process diverts the radical from free-radical reactivity into a catalytic cycle that governs bond formation.

Olefination/desaturation. In 2022, Rueping *et al.* reported a dual photoredox/cobaloxime catalysis that couples PCET-triggered C–C bond scission with acceptorless dehydrogenation, affording

 This journal is © The Royal Society of Chemistry 2026

Open Access Article. Published on 16 June 2026. Downloaded on 6/19/2026 2:50:40 PM. This article is licensed under a Creative Commons Attribution 3.0 Unported Licence.

olefins from aryl-bearing tertiary cycloalkanols with H_2 as the sole byproduct (see Scheme 5, step 2, 2C).[92b] The system requires Mes–Acr–Me^+ (E^* ≈ +2.06 V *vs.* SCE), $Co(dmgH)_2PyCl$, and 2,4,6-collidine. The excitation of the acridinium generates $Ar^{\bullet+}$ from the electron-rich arene, which, *via* a SET-MS-PCET with the alcohol and base, furnishes the **alkoxyl radical E**. β-scission yields a distal **alkyl radical F** that is trapped by Co(II), entering the cobalt cycle through alkyl–Co(III) intermediates that undergo Co–C homolysis and β-H abstraction to deliver the olefin and H_2. The choice of Mes–Acr–Me^+ is key, as its excited state oxidizes the arene while its reduced form reduces Co(III), thus synchronizing both catalytic cycles. This bioinspired strategy, reminiscent of enzymatic desaturations, established PCET-driven olefination as a powerful platform. Wu and co-workers soon broadened the scope to over 50 substrates, including natural product derivatives, confirming the robustness of this dual PC/Co system.[93] By contrast, Wu *et al.* later introduced a PC/Cu dual catalysis[94] that replaces direct PCET with *in situ* prefunctionalization. Thus, alcohols undergo ligand exchange with I(III) reagents (PIDA) to form O–I adducts, which are then reduced by Mes–Acr–$Me^\bullet$ to release alkoxyl radicals. This SET pathway circumvents the thermodynamic barrier of O–H activation and extends the reactivity to substrates lacking electron-rich arenes, including alkenes and alkynes.

Cross-coupling. The first dual PCET/transition-metal strategy for cross-coupling was introduced by Rueping *et al.* in 2020 with the remote arylation of ketones from tertiary cycloalkanols.[95] In this blueprint, *Mes–Acr–Me^+ engages in SET–MS-PCET with electron-rich arenes (*e.g.*, PMP) and 2,4,6-collidine, generating an **alkoxyl radical E** that undergoes β-scission to a distal **alkyl radical F**. Interception by Ni(0) gives an alkyl–Ni(I) intermediate, which proceeds *via* oxidative addition to an aryl halide and reductive elimination to furnish the coupled ketone. Closure of both catalytic cycles is achieved by SET reduction of Ni(I) with the reduced acridinium. This design demonstrated broad applicability but remained dependent on aryl substituents to mediate efficient SET–MS-PCET, limiting generality. A contribution from Xu and co-workers in 2022[96] retained the same SET–MS-PCET activation but redirected the **alkyl radical F** into hydroalkylation of alkynes. Interception of the F by Ni generates an alkyl–Ni(I) intermediate, which undergoes insertion into the alkyne to afford vinyl ketones with Markovnikov selectivity. This outcome reflects a key feature of radical/Ni relay catalysis, namely that rapid metal interception must outcompete alternative radical pathways to enforce selective C–C bond formation. Despite this conceptual advance, substrate scope remained limited, reflecting the continued reliance on electron-rich arenes for efficient radical initiation. A different trajectory was taken by Chang *et al.* in 2024, who coupled SET–MS-PCET with inner-sphere Ni–nitrenoid chemistry to achieve amidation.[97] Herein, the **alkyl radical F** engages a Ni–nitrenoid complex instead of a Ni(0) species. Reductive elimination from the resulting alkyl–Ni(III)–NR intermediate delivers the amide, while the reduced acridinium resets Ni(I) to Ni(0). Unlike aryl halide couplings, this manifold demands tight synchronization between radical generation and nitrene transfer, highlighting both the potential and fragility of extending PCET platforms to C–N bond formation.

In 2025, Scheidt and co-workers reported a transition-metal-free dual NHC/photoredox strategy for remote acylation of tertiary cycloalkanols, delivering 1,*n*-dicarbonyl scaffolds.[98] SET–MS-PCET activation from Mes–Acr–Me^+/2,4,6-collidine generates the **alkoxy radical E**, which undergoes β-scission to the **alkyl radical F**. Downstream functionalization proceeds through a persistence-selectivity regime rather than metal interception. In parallel, the NHC catalyst converts acyl precursors into acyl azoliums that are reduced by the photocatalyst to persistent ketyl radicals. Cross-coupling between the persistent ketyl radical and the transient **alkyl radical F** forges the $C(sp^3)$–$C(sp^2)$ bond, enabling remote acylation without oxidative addition or reductive elimination. Although conceptually distinct from metal-based relays, this platform remains constrained by stringent redox matching between the photoredox and NHC cycles and is currently limited to a narrow set of non-strained rings, with few genuine late-stage examples. In 2025, Zou, Huang, and co-worker reported a dual PC/chromium catalysis enabling enantioselective remote alkylation of tertiary cycloalkanols.[99] SET–MS-PCET activation generates the **alkoxy radical E**, and incorporation of an α-allyl substituent adjacent to the alcohol ensures that C–C bond cleavage furnishes a stabilized allyl radical F. This allyl radical is selectively intercepted by a chiral Cr(II)–bis(oxazoline) complex, triggering an RPC to a configurationally defined organochromium(III) species. In contrast to Ni or Co systems, where the metal mainly acts as a radical trap, the Cr center converts the open-shell intermediate into a nucleophilic organometallic reagent that engages aldehydes through a Zimmerman–Traxler-type transition state, enabling enantiocontrol. SET between the reduced acridinium PC and Cr(III) closes both catalytic cycles. While the scope remains restricted to allyl-substituted tertiary alcohols, this study illustrates how substrate electronics and chromium's redox flexibility can translate PCET-driven skeletal editing into enantioselective C–C bond formation, outlining a distinct blueprint for asymmetric organometallic reactivity.

3.3.3. Ligand-to-metal charge transfer (LMCT). Having examined PCET-based strategies for direct O–H bond activation, it is important to note that these processes operate through outer-sphere SET events within the framework of visible-light photoredox catalysis. Upon excitation, Ru(II) or Ir(III) complexes—or organic dyes— populate long-lived, non-dissociative excited states (typically MLCT or IL/ICT in character) that act as strong oxidants or reductants.[100] The alcohol, or its conjugate base, is oxidized *via* stepwise ET/PT or concerted PCET to generate the **alkoxy radical E**. However, because these are bimolecular processes, their efficiency depends on redox matching and the excited-state lifetime of the photocatalyst. This dependence often limits reactivity to tertiary or benzylic alcohols, where β-scission provides an additional driving force, leaving secondary alcohols challenging. A conceptually distinct solution arises from LMCT excitation, which offers a direct inner-sphere route to the same key intermediate.

Open Access Article. Published on 16 June 2026. Downloaded on 6/19/2026 2:50:40 PM. This article is licensed under a Creative Commons Attribution 3.0 Unported Licence.

In LMCT systems, the alcohol first coordinates to a high-valent metal centre, typically Ce(IV), Fe(III), or Ti(IV), forming a metal–alkoxide complex (M–OR). Light absorption promotes an electron from an oxygen-centred orbital (σ or π) of the alkoxide to an empty metal d orbital, generating a dissociative LMCT excited state in which the M–O bond order decreases dramatically. This state undergoes homolytic cleavage, producing **alkoxy radical E** and a reduced metal species (M^{n-1}) in a single photoinduced step (see Scheme 5, step 1B for a comparison between PCET and LMCT reactivity). Mechanistically, LMCT differs from photoredox PCET in key aspects. First, because the substrate is precoordinated, SET is intramolecular and does not depend on diffusional encounter or long-lived excited states, rendering activation fast even for electronically mismatched or sterically hindered alcohols. Second, the excited state is inherently dissociative, so bond cleavage occurs directly upon photoexcitation. Finally, the metal centre both anchors the substrate and provides the low-lying d orbitals required for charge transfer, enabling reactivity inaccessible to PCET catalysis.

These features explain why LMCT platforms can readily engage secondary or unactivated cycloalkanols, promoting selective β-scission and C–C bond cleavage even in the absence of an aryl redox handle or strong base. Moreover, the radicals generated under LMCT conditions often exhibit distinct chemoselectivity compared to those from PCET. Metals such as Ce, Fe, and Ti are ideally suited for this type of reactivity. Their high oxidation states and oxophilicity stabilize the M–OR precursors, while their low-lying d orbitals enable efficient ligand-to-metal excitation. Furthermore, their earth abundance, low toxicity, and broad photochemical tunability make them sustainable alternatives to Ru and Ir complexes. Together, these characteristics position LMCT catalysis as a powerful and complementary platform to PCET for light-driven O–H activation, capable of transforming inert alcohols into versatile radical intermediates under mild conditions. In the next sections we will discuss the different metals able to undergo LMCT to generate the alkoxy radicals on unstrained cyclic alcohols and subsequent functionalization.

Cerium systems. These constitute the earliest and most established LMCT platform for alkoxy radical generation from unstrained alcohols, from which subsequent systems have evolved. LMCT reactivity at cerium has been developed almost entirely by the group of Zuo, who reported the first example in 2016 using $CeCl_3$/Bu_4NCl under visible light.[101] Coordination of cyclic alcohols to Ce(III), followed by O → Ce excitation, triggers homolytic M–O cleavage to generate **alkoxy radical E**, which undergoes β-scission to a distal **alkyl radical F** and can be intercepted in C–N amination sequences (Scheme 6, 1B). This work established cerium-mediated LMCT as a viable platform for direct alkoxy radical generation from unstrained cyclic alcohols. A key limitation, however, arises from the narrow redox window of the Ce(IV)/Ce(III) couple ($E_{1/2} \approx +0.4$ V *vs.* SCE in MeCN). As a result, catalytic turnover becomes challenging in manifolds requiring net reduction, particularly Giese-type alkylation pathways, where the post-addition alkyl radicals are insufficiently reducing to regenerate Ce(III) and close the catalytic cycle. To overcome this redox mismatch, the Zuo group subsequently introduced a dual-photocatalytic strategy.[102] In this manifold, LMCT at Ce(III) generates an **alkoxy radical E** that undergoes rapid β-scission to a nucleophilic **alkyl radical F**, which engages in Giese-type addition to electron-deficient alkenes, including under flow conditions. The resulting α-acyl radical ($E_{1/2} \approx -0.60$ V *vs.* SCE) lies outside the Ce(III)/Ce(IV) redox window but is efficiently reduced by photoexcited 9,10-diphenylanthracene (DPA; $E^* \approx -1.77$ V *vs.* SCE), delivering an enolate intermediate. Oxidized DPA then returns an electron to Ce(III), closing both catalytic cycles, and intramolecular cyclisation furnishes ring-expanded products. Overall, this sequence constitutes an LMCT-enabled ring expansion *via* Giese addition followed by cyclisation. Notably, the introduction of DPA as a redox mediator established a general strategy to bypass intrinsic metal redox limitations, later adopted broadly in LMCTCh-based photochemistry.

A significant conceptual advance came with the extension of LMCT to cyclic ketones.[55] *In situ* conversion of cyclic ketones into cyanohydrin–$TiCl_4$ adducts allowed formation of Ce(IV)–O complexes that, upon LMCT excitation, generated **alkoxy radical E** able to cleave the α-C–C bond and generate the distal **alkyl radical F**. The subsequent fate of the radicals is strongly ring-size dependent. In cyclobutanones and cyclopentanones, **alkyl radicals F** undergoes intramolecular addition to the acyl cyanide, triggering cyanide migration through five- or six-membered cyclic intermediates to generate nucleophilic carbonyl radicals and rearranged carbonyl products. In contrast, for six-membered and larger cyclic ketones, as well as acyclic systems, intramolecular cyanide migration becomes entropically disfavored, and the **alkyl radicals F** is instead intercepted intermolecularly, followed by single-electron reduction to afford ring-opened cleavage products. Carbonyl activation remains uncommon across PCET, LMCT, and FRP platforms, as ketones lack an O–H handle and do not readily form metal–alkoxide complexes without derivatization. By accessing Ce–O species through cyanohydrin formation, this study bypassed that limitation and enabled direct α-C–C cleavage in ketones, a reactivity mode that remains difficult to access under any of these activation manifolds. Subsequent studies further showed that LMCT can proceed through either Ce–OR or Ce–Cl excitation depending on the ligation environment, generating $RO^•$ or $Cl^•$ as the initiating species.[103] Both pathways promote β-scission in hemiacetals, although their coexistence complicates assignment of the radical species responsible for bond cleavage and selectivity.

Iron systems. Iron complexes have emerged as adaptable platforms for generating **alkoxyl radicals E** from unstrained five- and six-membered cyclic alcohols. A consistent theme across these systems is that small changes in the ligand environment control which ligand undergoes LMCT, thereby defining whether $Cl^•$ or $RO^•$ initiates β-scission. The chronological development of these platforms illustrates how the coordination sphere dictates both scope and downstream reactivity.

 This journal is © The Royal Society of Chemistry 2026

Open Access Article. Published on 16 June 2026. Downloaded on 6/19/2026 2:50:40 PM. This article is licensed under a Creative Commons Attribution 3.0 Unported Licence.

The earliest contributions employed chloride-based LMCT from $FeCl_4^-$. In 2021, the Hu group showed that blue-light LMCT from $FeCl_4^-$ generates Cl•, which abstracts the O–H hydrogen of alcohols to give **alkoxy radical E**. After β-scission, the resulting **alkyl radical F** undergoes HAT-based termination, accounting for the formation of carbonyl products from tertiary and secondary cyclic alcohols (Scheme 6, 1A, HAT process).[104] One year later, the same group showed that the β-scission radicals undergo Giese-type addition to electron-deficient alkenes, enabling deconstructive alkylation of unstrained rings bearing aryl or methyl substituents.[105] These studies established Cl-initiated RO• formation as a general entry point but also highlighted its sensitivity to HAT selectivity. A mechanistic shift occurred when Zeng and co-workers introduced direct Fe–OR LMCT under strongly basic $Fe(acac)_3$/*t*BuONa conditions in 2022 (Scheme 6, 1A, external SOMOphiles).[106] In this case, **E** is generated directly from Fe–OR without participation of Cl•, suppressing competing HAT pathways. This enabled ring-opening bromination of tertiary cyclic alcohols bearing arenes, although the requirement for strong base limited compatibility with electrophilic acceptors and substrates sensitive to basic media. To address these constraints, Liu and co-workers developed a neutral $FeCl_3$/TBACl system in which Fe–Cl/Fe–OR LMCT operates under milder conditions.[107] This work allows two types of deconstructive/functionalization reactions: (i) amination and (ii) alkylation. In the deconstructive amination with dibenzyl azodicarboxylate (DBAD), the β-scission carbon-centred radical is directly trapped by the azo acceptor, following a pathway analogous to earlier Ce-OR LMCT-based protocols (see work of Zuo). For deconstructive alkylation, DPA is introduced as a co-catalyst: after Cl-based LMCT and β-scission, the **alkyl radical F** undergoes Giese-type addition to an electron-deficient alkene, and the resulting radical is reduced to the corresponding carbanion by SET from DPA, followed by protonation from the medium.

Vanadium systems. In 2023, Soo, Ramalingam, and co-workers disclosed a vanadium photocatalytic platform that enables direct deconstructive functionalization of unactivated aliphatic alcohols under visible light *via* inner-sphere LMCT.[16a] In this manifold, the alcohol first forms a V–OR adduct, and photoexcitation triggers a dissociative LMCT event within the coordination sphere, leading to C–C bond cleavage without requiring outer-sphere oxidation of the substrate. A key mechanistic feature is that the V(v)/V(iv) redox couple is not sufficiently oxidizing to convert alkoxides into freely diffusing alkoxy radicals ($V^V/V^{IV} \leq +0.30$ V *vs.* Fc^+/Fc, as discussed by the authors in the context of their earlier mechanistic work).[108] Consequently, in contrast to Ce- and Fe-based LMCT platforms that can access alternative activation pathways depending on oxidation state and ligation, vanadium enforces a strictly inner-sphere process in which the coordinated alcohol undergoes photoinduced reorganization and β-scission to generate a nucleophilic carbon-centered radical, subsequently intercepted by suitable radical acceptors (“SOMOphiles”; Scheme 6, 1A). This mechanistic constraint translates into broad substrate coverage, spanning acyclic alcohols and unstrained 4–8-membered rings, and into high modularity after scission. The same radical-forming step can be coupled to oxidative, redox-neutral, or reductive termination modes, enabling diverse bond constructions in a single platform. As in Ce- and Fe-based systems, multiple downstream manifolds can be accessed from the common radical intermediate; for example, Giese-type alkylations to electron-deficient alkenes (*e.g.*, –CN or $-SO_2Ph$ substituted) employ DPA as an auxiliary electron shuttle. Beyond C–C bond formation, this vanadium LMCT platform supports a wide range of transformations, including C–Br, C–N, C–S, C–Se, C–H, C–D, and C–O bond formation. Its generality is underscored by late-stage modification of structurally complex substrates and natural products, such as L-menthol and diosgenin, highlighting the relevance of vanadium-based LMCT for skeletal editing of unstrained alcohols under mild photochemical conditions.

Titanium systems. Ti(iv)–alkoxide complexes also undergo LMCT, but operate in a distinct regime in which reversible C–C bond activation is followed by enantioselective reclosure, leading to enantioenrichment rather than deconstructive functionalization. In 2023, Zuo *et al.* reported the photoexcitation of chiral Ti(iv)–alkoxide complexes induced O → Ti LMCT, generating alkoxy radicals that undergo β-scission of adjacent C–C bonds.[109] The key mechanistic distinction of this system lies in the fate of the resulting radical pair. Following C–C cleavage, a carbon-centred radical and a Ti(iii)-bound carbonyl fragment are generated in close proximity within the same coordination environment (see Scheme 6, 1D). Unlike Ce-, Fe-, or V-based LMCT platforms, where the alkyl radical is rapidly trapped or driven into irreversible redox processes, the Ti system operates under redox conditions that do not promote radical escape or outer-sphere electron transfer. As a result, recombination of the cleaved fragments becomes kinetically competitive and ultimately dominant. Importantly, reclosure of the C–C bond occurs under the control of the same chiral Ti complex that mediates LMCT, typically ligated by chiral phosphate or bisoxazoline ligands. This enables selective re-formation of the C–C bond from a planar, prochiral radical intermediate, leading to efficient deracemization of adjacent stereocenters. Although neither the cleavage nor the recombination step is fully enantioselective on its own, the sequential operation of both processes results in high overall enantioenrichment. From a broader perspective, this chemistry demonstrates that LMCT-induced alkoxy radical formation does not necessarily imply irreversible skeletal editing. When radical diffusion and downstream trapping are suppressed by coordination and redox balance, LMCT can instead enable reversible C–C bond activation and stereochemical editing. In this sense, titanium occupies a distinct mechanistic niche among LMCT-active metals, illustrating how modulation of redox strength and metal–substrate association can redirect alkoxy-radical chemistry away from functionalization and toward dynamic control of molecular chirality.

Open Access Article. Published on 16 June 2026. Downloaded on 6/19/2026 2:50:40 PM. This article is licensed under a Creative Commons Attribution 3.0 Unported Licence.

Electrophotochemical (EPC) metal catalysis. While PCET- and LMCT-based strategies have firmly established that cyclic alcohol fragmentation can be coupled to alkylation processes, most commonly *via* Giese-type addition to electron-deficient alkenes (Scheme 6, 1B), extension to arylative C–C bond formation has proven substantially more demanding (Scheme 6, 1C). Construction of aryl–alkyl bonds requires interception of the alcohol-derived alkyl radical by a cross-coupling manifold rather than simple radical addition. In this context, nickel catalysis is uniquely suited, as Ni efficiently captures unstabilised alkyl radicals and enables $C(sp^3)$–$C(sp^2)$ bond formation through Ni(I)/Ni(III) cycles with aryl halides. Productive turnover, however, requires access to low-valent Ni species (Ni(0)/Ni(I)), whose redox couples typically lie in the range Ni(II)/Ni(I) ≈ -0.6 to -1.2 V *vs.* SCE, depending on ligand environment. Under these conditions, Ni catalysis is highly sensitive to strongly oxidizing environments. By contrast, alkoxy radical generation *via* dissociative LMCT generally requires highly oxidizing photoactive metal–ligand states, which are incompatible with sustaining low-valent Ni intermediates within a single closed redox manifold. As a result, while alkylation pathways are readily accessible, Ni-mediated arylation of cyclic alcohol fragments remained elusive under LMCT conditions. The relevance of Ni cross-coupling in this context was first demonstrated in 2020 by Rueping and co-workers using PCET activation of electronically activated alcohols, where alkoxy radical formation and Ni turnover could be accommodated within the same photoredox window (Scheme 6, 1C).[95] By contrast, LMCT-based activation modes did not enable deconstructive arylation of cyclic alcohols until 2024, as the oxidative requirements of LMCT conflicted with the need to maintain Ni in low oxidation states necessary for oxidative addition and $C(sp^3)$–$C(sp^2)$ bond formation. This redox incompatibility motivated the development of electrophotochemical (EPC) and photoelectrochemical strategies, in which radical generation and cross-coupling are decoupled by external electrochemical bias. In 2022, Lei and co-workers introduced electrophotochemical cerium catalysis for ring-opening functionalization of cyclic alcohols.[110] In this approach, EPC bias controls the Ce redox state, while photoexcitation enables alkoxy radical formation and β-scission under overall redox-neutral conditions, allowing modulation of radical fate toward C–CN, C–C, or C–heteroatom bond formation. Subsequent EPC studies focused mainly on strained cyclobutanol derivatives, where anodic control enables ring contraction and functionalisation.[111]

Extension to Ni-catalyzed arylation of unstrained cyclic alcohols was achieved in 2024 through dual Fe/Ni platforms (Scheme 6, 1C). Amgoune and co-workers reported a purely photochemical Fe/Ni system in which LMCT excitation of Fe–halide complexes generates alkoxy radicals E, followed by β-scission and interception of the resulting linear radicals by Ni to afford deconstructive arylation of five- and six-membered cyclic alcohols.[112] In this system, DPA is required to maintain productive turnover of both the Fe-LMCT and Ni catalytic cycles. By contrast, in 2024 the group of Lu developed an EPC/Fe/Ni system in which radical generation is controlled anodically and Ni-catalyzed $C(sp^3)$–$C(sp^2)$ coupling is sustained cathodically, eliminating the need for an organic redox mediator.[113] Although both approaches employ similar catalytic components ($FeCl_3$ and $NiCl_2$·DME), their scope differs: the EPC system is largely limited to aryl bromides bearing electron-withdrawing substituents compatible with electroreductive conditions, whereas the purely photochemical Fe/Ni platform tolerates a broader range of aryl bromides regardless of their electronic properties. In addition, in 2024, Mei and co-workers reported a related Ni-mediated arylation of unstrained cyclic alcohols using visible-light photocatalysis assisted by paired electrolysis, in which the electrochemical input primarily serves to sustain catalyst turnover rather than to introduce a distinct activation or coupling manifold.[114]

3.3.4. Frustrated radical pairs (FRPs). Frustrated radical pairs (FRPs) provide an alternative entry to alkoxy radical generation that does not rely on PCET manifolds or LMCT processes (see Scheme 5, step 1C). In the context of alcohol activation, the FRP exists only at the level of O–H bond cleavage and involves a persistent oxidizing radical, typically a nitroxyl species, and a nascent alkoxy radical generated upon deprotonation and SET. This activation step is intrinsically redox-biased, as the alcohol must act as a reductant toward the persistent radical partner, enabling O–H activation without invoking excited states or metal coordination. While this activation logic has been exploited in selective aliphatic C–H functionalization (Frustrated radical pairs in selective functionalization of inert aliphatic C–H bonds),[115] its application to skeletal editing, particularly to the deconstruction of unstrained cyclic alcohols, has only recently been demonstrated. To date, only one FRP-enabled example of alkoxy radical–induced C–C bond cleavage in unstrained cyclic alcohols has been reported.[116] In this work, the group of Lin reported that an *in situ* FRP is formed between a sterically hindered nitroxyl radical (TEMPO-derived) and the cyclic alcohol substrate, generating an **alkoxy radical E** that undergoes rapid β-scission to afford a distal **alkyl radical F**. At this stage, productive functionalization is limited to recombination with the nitroxyl partner, yielding O–TEMPO adducts ($C(sp^3)$–OTEMPO) (see Scheme 6, 1A as external SOMOphiles example of radical trapping approach). Other transformations reported in this study rely on subsequent postfunctionalization of these aminoxyl products rather than direct interception of the carbon-centred radical. The alkyl radical generated after C–C bond cleavage does not engage in a second frustrated radical pair; instead, radical termination *via* TEMPO trapping is kinetically dominant, confining FRP character to the alkoxy radical generation step and preventing propagation into downstream radical chemistry.

In this sense, the absence of a second FRP regime after C–C bond cleavage reflects intrinsic requirements of FRP chemistry rather than limitations of substrate design. In the reported system, FRP character is confined to the O–H activation step, which is enabled by a defined redox asymmetry between the nitroxyl oxidant and the alcohol-derived reductant. After β-scission, the resulting carbon-centred radicals are neutral

 This journal is © The Royal Society of Chemistry 2026

Open Access Article. Published on 16 June 2026. Downloaded on 6/19/2026 2:50:40 PM.
This article is licensed under a Creative Commons Attribution 3.0 Unported Licence.

alkyl or acyl species and do not sustain the redox imbalance necessary to engage in a secondary alkyl–nitroxyl FRP. Consequently, interception by the nitroxyl partner is kinetically dominant. Across the substrate scope, β-C–C bond cleavage follows conventional radical stability trends, favouring secondary over primary radicals (*e.g.*, camphor derivative, 90% yield, r.r. = 2.5 : 1) and more substituted radicals in fused systems (estrone derivative, 53% yield, d.r. = 7.8 : 1). The generation of acyl radicals represents a genuine expansion of the radical manifolds accessible through FRP initiation; however, these intermediates are likewise captured as aminoxyl derivatives, and productive functionalization remains limited to TEMPO recombination.

From a design perspective, advancing FRP-based skeletal editing beyond termination-controlled outcomes will require strategies that suppress nitroxyl trapping. This may involve alternative persistent radicals with reduced recombination kinetics, faster orthogonal interception of the carbon-centred radical, or temporal separation of FRP-mediated O–H activation from downstream capture. Addressing these constraints defines the key challenge for extending FRPs from activation tools to diversification platforms in skeletal editing.

3.3.5. Miscellaneous. Several isolated strategies fall outside the dominant activation paradigms discussed above but are worth brief mention for their conceptual originality. In 2015, Lectka and co-workers reported a C–C fragmentation/fluorination of 1,4-dioxaspiro[4.5]decane,[117] distinct from the spirocyclic aminium radical manifolds discussed earlier. In this case, the presence of an aryl substituent was proposed to stabilize a putative radical cation sufficiently to enable productive C–C cleavage, ultimately manifesting as a strategy for remote fluorination of carboxylic acid derivatives. Related but mechanistically distinct behavior is observed when carboxylic acids are used as radical precursors. In 2022, Xia and co-workers developed an Fe-catalyzed, photoinduced LMCT protocol for the decarboxylative ring opening of cyclic tertiary carboxylic acids.[118] Mechanistic studies support oxygen capture to form peroxy radical species, followed by radical fragmentation, highlighting a pathway in which C–C cleavage is coupled to oxidative radical processes rather than alkoxy radical β-scission. More recently, Hari and co-workers reported an electrochemical interrupted Dowd–Beckwith reaction enabling deconstructive functionalization of cyclic ketones.[12] In this system, reductive decarboxylation at the anode generates a primary alkyl radical that can undergo further oxidation to a carbocation, triggering β-fragmentation to give acylium ions and terminal alkenes, or less favorably acyl radicals. Ring expansion pathways were also observed but remained minor, illustrating how electrochemical control can unlock alternative fragmentation manifolds. In 2025, Zhang, Jin, and Zuo reported a conceptually distinct entry point in which skeletal editing is initiated from an alkene rather than from a pre-existing alcohol or a derivatized carbonyl.[119] Building on their earlier work,[120] a highly oxidizing bisphosphonium photocatalyst (BPP; $E^{*}_{1/2} \approx +2.17$ V *vs.* SCE) enables SET oxidation of cycloalkenes to alkene radical cations, which undergo anti-Markovnikov hydration to afford secondary alcohol intermediates. Crucially, the electron-rich arene required for oxidation is positioned on the adjacent carbon rather than on the alcohol-bearing center, enabling a long-range, arene-mediated MS-PCET event that generates the **alkoxy radical E** without the need for direct aryl substitution at the O–H carbon. This design allows efficient β-scission of secondary alcohols, overcoming a key limitation of previous MS-PCET and SET-based approaches. Ring opening is followed by HAT to deliver distal aldehyde products under overall redox-neutral conditions, with thiol-based donors currently required to buffer the high oxidizing power of BPP and enable clean catalyst turnover. More broadly, this work illustrates how alkene activation can serve as a versatile gateway to alkoxy radical chemistry, opening new design space beyond established LMCT, MLCT, FRP, and oxime-based strategies. In our view, this study plants an important seed for the field: by moving away from O–H and C═O-centred entry points and using alkenes as the gateway, it offers a more accessible and less prerequisite-driven route to skeletal editing, although expanding functional group compatibility beyond thiol-mediated HAT will likely require future strategies to decouple oxidation from downstream radical interception.

4. C–C bond cleavage: expansion

Ring expansion has been predominantly developed through C–C bond cleavage. The dominant approach is based on bicyclic or bridged functional groups, in which the radical intermediate participates in a Dowd–Dowd-Beckwith-type process. In this context, two main strategies have been developed. The first strategy involves ring expansion triggered by the generation of an **alkoxy radical E**, which is strategically embedded within a bicyclic framework (see Scheme 7). As a consequence, the **alkyl radical F** generated upon β-scission evolves into a macrocyclic, rather than an acyclic intermediate, as discussed above. Accordingly, **F** remains confined within a macrocyclic or lactone architecture. In this strategy, bicyclic peroxides or tertiary alcohols serve as alkoxy radical precursors *via* LMCT or PCET pathways.[121] In addition, ketones capable of generating an *in situ* Ce–O species embedded within a bicyclic framework have also been employed.[122] A second strategy relies on decarboxylative Dowd–Dowd-Beckwith-type processes (see Scheme 7). In this case, rather than a bicyclic alkoxy radical precursor, primary alkyl radicals are generated from carboxylate precursors, enabling subsequent rearrangement and ring expansion within an already constrained scaffold.[123] Alongside Dowd–Dowd-Beckwith-derived expansion manifolds, ring expansion has also been achieved through strategies that exploit MS-PCET activation of cyclic alcohols, as discussed above for secondary alcohol homolysis. In this context, Knowles and co-workers applied the same hydrogen-bond-assisted MS-PCET platform to cyclic aminoalcohols to enable skeletal reorganization (see Scheme 1 part D).[124] In this work, MS-PCET-mediated O–H homolysis forms an **alkoxy radical E** that undergoes regioselective C–C β-scission, with selectivity governed by cleavage pathways leading to energetically accessible,

Open Access Article. Published on 16 June 2026. Downloaded on 6/19/2026 2:50:40 PM.
This article is licensed under a Creative Commons Attribution 3.0 Unported Licence.

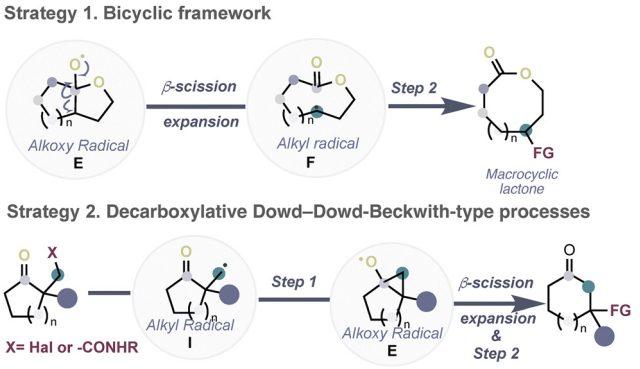

Scheme 7 Strategies for ring expansion *via* radical β-scission pathways.

geometrically primed open-chain radicals for rapid intramolecular reclosure. Operating under redox-neutral conditions, the resulting radical manifold disfavors intermolecular interception and instead converts exocyclic amines into endocyclic *N*-heterocycles through net skeletal reorganization.

5. C–N bond cleavage

This section does not seek to comprehensively survey C–N bond cleavage in saturated heterocycles, but rather to frame how C–N scission has been incorporated into recent skeletal editing strategies. The focus is placed on approaches where bond cleavage is intrinsically coupled to controlled framework reorganization, rather than treated as an isolated disconnection. Historically, C–N bond cleavage in unstrained cyclic amines has been dominated by polar or metal-mediated processes, typically proceeding through oxidative activation or electrophilic von Braun-type pathways that result in ring opening.[19a] Translating C–N scission into the radical area is inherently challenging, as it requires transient weakening of a robust σ C–N bond in the absence of ring strain. The feasibility of such processes is highly dependent on the nitrogen functionality, with amides and amines displaying distinct electronic responses under reducing conditions.[20a,b]

Deconstruction/functionalization

In *N*-acyl cyclic amines, the C(acyl)–N bond is reinforced by $n_N \rightarrow \pi^*_{CO}$ conjugation, rendering reductive activation possible but demanding. Procter and co-workers demonstrated that this barrier can be overcome under strongly reducing conditions using lanthanide(II) iodides ($E^\circ \approx -2.6$ V *vs.* SCE), where carbonyl reduction generates a ketyl-type radical anion that disrupts amide conjugation and enables C–N bond scission, leading to ring opening and radical termination pathways *via* HAT.[13b] Related photoredox strategies have since replaced stoichiometric reductants with highly reducing organic photocatalysts, enabling catalytic ring opening of *N*-acyl cyclic amines under visible light, albeit still under strongly reducing regimes.[13c] A recurring limitation of these approaches lies in the restricted scope of downstream functionalization. The alkyl radicals generated upon C–N cleavage are often more readily reduced than the parent amides, favoring over-reduction to carbanions and confining reactivity to anionic manifolds. This inherent bias complicates the development of skeletal editing strategies in which bond scission is followed by controlled refunctionalization. In this context, the work of Yamaguchi and co-workers provide a distinct conceptual advance by enabling radical-mediated deconstruction of non-strained cyclic amides under catalytic conditions while maintaining control over post-cleavage reactivity (see Scheme 1, part C).[21a] Although amide reduction typically lies beyond the reach of standard photocatalysts, aromatic amides exhibit comparatively less negative reduction potentials ($E_{1/2} \approx -2.3$ V *vs.* SCE), rendering them accessible under dual photoredox and Lewis acid catalysis. Coordination of $Zn(OTf)_2$ facilitates SET reduction to an aminoketyl radical, whose β-scission constitutes the decisive C–N cleavage step. The resulting alkyl radical is subsequently directed into productive pathways, including HAT and Giese-type additions. The addition to terminal alkenes can proceed through SET oxidation followed by HAT, while intramolecular SET oxidation and cyclization enable lactone formation. Alternatively, alkene functionalization can occur *via* extrusion of an aryl sulfonyl radical. In addition, interception with alkynes furnishes styrene derivatives from pyrrolidine precursors.

Ring contraction represents the most clearly delineated application of skeletal editing enabled by C–N bond cleavage in unstrained nitrogen heterocycles. Its defining feature is that C–N scission does not manifest as a free ring-opening event, but is embedded within reaction manifolds that kinetically enforce rapid framework reorganization. This principle was established in the photomediated ring contraction of α-acylated saturated heterocycles reported by Sarpong and co-workers (see Scheme 1, part C top view). A Norrish type II excitation of a pendant carbonyl triggers intramolecular HAT, generating a short-lived radical manifold in which C–N bond fragmentation competes and is immediately followed by intramolecular C–C bond formation to afford a smaller carbocyclic framework.[5c] From a synthetic standpoint, the key advance is not the activation of the C–N bond itself, but the temporal coupling of bond cleavage with reclosure, which suppresses diffusional ring opening and irreversible deconstruction of the heterocycle. Subsequent mechanistic studies clarified that contraction efficiency is governed by the photophysical entry point and by conformational control of the post-HAT intermediate, rather than by intrinsic C–N bond weakness. Systematic variation of excitation wavelength, *N*-substituent electronics, and intramolecular hydrogen bonding revealed how these factors modulate the lifetime and geometry of the imine–enol radical pair generated after C–N scission, thereby dictating the balance between productive contraction and competing back-HAT or fragmentation pathways.[125] Importantly, later work demonstrated that stereochemical information can be introduced at the reclosure stage, confirming that the decisive selectivity-determining step occurs after bond cleavage but before conformational equilibration of the open intermediate.[126] The importance of these findings becomes clearer when contrasted with other modes of C–N bond cleavage in unstrained systems. In reductive photoredox strategies for amide C–N scission,

 This journal is © The Royal Society of Chemistry 2026

Open Access Article. Published on 16 June 2026. Downloaded on 6/19/2026 2:50:40 PM.
This article is licensed under a Creative Commons Attribution 3.0 Unported Licence.

bond cleavage can be achieved chemically but often leads to uncontrolled downstream reactivity unless additional constraints are imposed, underscoring the challenge of converting C–N cleavage into contraction when the fate of the resulting radical is not kinetically channelled.[21a] Conceptually related, but mechanistically distinct, approaches to ring contraction have also been developed for aromatic nitrogen heterocycles, most notably the photochemical net carbon deletion of azaarenes reported by Levin and co-workers, where selective excitation of quinoline *N*-oxides enables dearomative rearrangement followed by rearomatization with formal loss of a skeletal carbon atom.[127] Although this transformation does not involve C–N scission in saturated frameworks, it reinforces the same design principle: contraction becomes viable only when excitation selectively accesses a reactive manifold while suppressing secondary photochemical degradation.

Taken together, these studies explain why ring contraction has emerged as an important point within skeletal editing. It constitutes a rare scenario in which C–N bond cleavage can be rendered synthetically productive, not by weakening the bond or stabilizing the fragments, but by controlling the lifetime, geometry, and downstream fate of the post-scission intermediate through photochemical and conformational design.

Conclusions

This Tutorial Review has analysed radical-promoted skeletal editing as a strategy to fragment cyclic scaffolds primarily through C–C bond cleavage, with only a limited number of cases involving C–N bond scission. Rather than compiling individual transformations, the chemistry has been examined from a unified design perspective, in which unstrained rings become editable only after the deliberate introduction of appropriate radical gateways. Across the systems discussed, skeletal editing does not originate from the intrinsic reactivity of the ring framework, but from strategies that enable controlled backbone fragmentation followed by either reclosure or interception of the resulting radical intermediates. From this standpoint, cyclic alcohols emerge as the most direct and general class of gateways, as alkoxy radicals undergo rapid β-scission once generated. The review depicts multiple activation strategies that enable access to these intermediates, including PCET, LMCT, EPC variants, and FPRs manifolds. Although these approaches differ in how alkoxy radicals are formed, they converge on common post-scission carbon-centred radicals, whose fate is dictated by subsequent interception pathways. Cyclic ketones, by contrast, rarely undergo direct C–C bond cleavage and typically require prefunctionalisation to access productive radical manifolds, most commonly through oxime-derived iminyl radicals or pre-aromatic intermediates, where fragmentation is coupled to nitrile formation or aromatization. Only isolated cases bypass this requirement, and even these ultimately rely on the transient conversion of the ketone into an alcohol-type gateway. Strategies for C–N bond cleavage are comparatively fewer and more heterogeneous, reflecting the absence of a general radical gateway for saturated *N*-heterocycles despite their prevalence in bioactive molecules. Once fragmentation has occurred, skeletal editing diverges according to the use of the ring-opened radical. In some systems, recombination leads to new ring closures, enabling contraction or expansion processes; particularly notable are the limited examples in which reclosure is rendered enantioselective, demonstrating that backbone reorganization and stereochemical control can be coupled. In other cases, the radical is intercepted rather than re-cyclized, and the chemistry reviewed highlights a small number of interception modes that recur across methodologies. Giese-type additions constitute the most characteristic and widely exploited pathway, complemented by radical trapping, radical–polar crossover processes, and dual catalytic manifolds, particularly for cross-coupling reactions. While most studies focus on establishing methodological feasibility, a smaller number apply these concepts to late-stage skeletal editing of natural products and complex molecules, illustrating how backbone fragmentation and reconstruction can be integrated into advanced synthetic settings.

Taken together, the chemistry analyzed here provides a framework for designing deconstruction–construction sequences in skeletal editing, while also delineating the current boundaries of the field. General solutions for C–N bond cleavage in saturated heterocycles remain scarce, and enantioselective skeletal editing is still confined to isolated examples. Beyond these established strategies, the analysis also invites consideration of yet developed conceptual extensions. In this sense, although dearomatization and skeletal fragmentation have largely performed as separate areas, one may envisage combining dearomatization as a preparative step with subsequent fragmentation and functionalization. Such a sequence would amount to the complete dismantling of an aromatic ring within a skeletal editing framework. At present, this idea remains speculative, but it highlights how viewing bond cleavage and reconstruction together can reveal unexplored directions for backbone reprogramming.

Author contributions

The manuscript was written through the contributions of all authors. All authors have approved the final version of the manuscript. José Justicia: conceptualization, writing – original draft, review & editing; Sara P. Morcillo: conceptualization, project administration, supervision, funding acquisition, writing – original draft, review & editing.

Conflicts of interest

There are no conflicts to declare.

Abbreviations

BDE	Bond dissociation energy
BDFE	Bond dissociation free energy

Open Access Article. Published on 16 June 2026. Downloaded on 6/19/2026 2:50:40 PM. This article is licensed under a Creative Commons Attribution 3.0 Unported Licence.

CF_3	Trifluoromethyl
CPET	Concerted proton–electron transfer
DFT	Density functional theory
DME	1,2-Dimethoxyethane
DPA	9,10-Diphenylanthracene
EDA	Electron donor–acceptor
EBX	Ethynylbenziodoxolone
EPC	Electrophotochemical
ET	Electron transfer
Fc/Fc^+	Ferrocene/ferrocenium
FRP	Frustrated radical pair
HAT	Hydrogen atom transfer
ICT	Intramolecular charge transfer
IL	Intraligand
LMCT	Ligand-to-metal charge transfer
MLCT	Metal-to-ligand charge transfer
Ms-PCET	Multisite proton-coupled electron transfer
NHC	N-heterocyclic carbene
PCET	Proton-coupled electron transfer
PT	Proton transfer
PSS	Photostationary state
RPC	Radical–polar crossover
SCE	Saturated calomel electrode
SET	Single-electron transfer
SH_2	Homolytic substitution
SOMO	Singly occupied molecular orbital
TEMPO	(2,2,6,6-Tetramethylpiperidin-1-yl)oxyl

Data availability

No new experimental data, software or code were generated or analysed as part of this review.

Acknowledgements

This work was supported by grant PID2023-146433NB-I00 funded by MICIU/AEI/10.13039/501100011033 and by ERDF/EU. We also acknowledge support from Junta de Andalucía – Consejería de Universidad, Investigación e Innovación – Proyecto (P21_00133).

Notes and references

1 (*a*) J. B. Roque, Y. Kuroda, L. T. Göttemann and R. Sarpong, *Nature*, 2018, **564**, 244–248; (*b*) J. B. Roque, Y. Kuroda, L. T. Göttemann and R. Sarpong, *Science*, 2018, **361**, 171–174; (*c*) Y. Xu, X. Qi, P. Zheng, C. C. Berti, P. Liu and G. Dong, *Nature*, 2019, **567**, 373–378; (*d*) A. J. Smaligo, M. Swain, J. C. Quintana, M. K. Tan and O. Kwon, *Science*, 2019, **364**, 681–685; (*e*) C. Ma, C. W. Lindsey, J. Chan and B. Yu, *J. Med. Chem.*, 2024, **67**, 11459–11466; (*f*) N. J. Castellano, A. P. Montgomery, J. J. Danon and M. Kassiou, *Chem. Rev.*, 2023, **123**, 8127–8153; (*g*) M. Peplow, *Nature*, 2023, **618**, 21–24; (*h*) J. Jurczyk, J. Woo, S. F. Kim, B. D. Dherange, R. Sarpong and M. D. Levin, *Nat. Synth.*, 2022, **1**, 352–364; (*i*) K. R. Campos, P. J. Coleman, J. C. Alvarez, S. D. Dreher, R. M. Garbaccio, N. K. Terrett, R. D. Tillyer, M. D. Truppo and E. R. Parmee, *Science*, 2019, **363**, eaat0805.

2 H. J. Böhm, A. Flohr and M. Stahl, *Drug Discovery Today: Technol.*, 2004, **1**, 217–224.

3 (*a*) S. P. Morcillo, *Angew. Chem., Int. Ed.*, 2019, **58**, 14044–14192; (*b*) X. Wu and C. Zhu, *Chin. J. Chem.*, 2019, **37**, 171–182; (*c*) P. Sivagure, Z. Wang, G. Zanonia and Z. Bi, *Chem. Soc. Rev.*, 2019, **48**, 2615–2656.

4 P. Bhutani, G. Joshi, N. Raja, N. Bachhav, P. K. Rajanna, H. Bhutani, A. T. Paul and R. Kumar, *J. Med. Chem.*, 2021, **64**, 2339–2381.

5 (*a*) S. H. Kenndey, B. D. Dherange, K. J. Berger and M. D. Levin, *Nature*, 2021, **593**, 223–227; (*b*) W. Liu, Z. Wang, G. Wang, Q. Zeng, W. He, L. Liu, X. Wang, Y. Xi, H. Guo, C. Hu and Z. L. Wang, *Nat. Commun.*, 2020, **11**, 1883; (*c*) J. Jurczyk, M. C. Lux, D. Adpressa, S. F. Kim, Y. Lam, C. S. Yeung and R. Sarpong, *Science*, 2021, **373**, 1004–1012.

6 (*a*) C. K. Prier, D. A. Rankic and D. W. C. MacMillan, *Chem. Rev.*, 2013, **113**, 5322–5363; (*b*) N. A. Romero and D. A. Nicewicz, *Chem. Rev.*, 2016, **116**(17), 10075–10166; (*c*) X. Y. Yu, J. R. Chen and W. J. Xiao, *Chem. Rev.*, 2021, **121**, 506–561.

7 E. C. Gentry and R. R. Knowles, *Acc. Chem. Res.*, 2016, **49**, 1546–1556.

8 Selected reviews: (*a*) R. Zhao and L. Shi, *Org. Chem. Front.*, 2018, **5**, 3018–3021; (*b*) Y. Yang, X. Huang and Y. Jin, *Chem. Commun.*, 2025, **61**, 1944–1961.

9 (*a*) L. Capaldo, D. Ravelli and M. Fagnoni, *Chem. Rev.*, 2022, **122**, 1875–1924; (*b*) F. Juliá, T. Constantin and D. Leonori, *Chem. Rev.*, 2022, **122**, 2292–2352; (*c*) G. E. M. Crisenza, D. Mazzarella and P. Melchiorre, *J. Am. Chem. Soc.*, 2020, **142**, 5461–5476.

10 (*a*) K. Khoury, M. K. Sinha, T. Nagashima, E. Herdtweck and A. Dömling, *Angew. Chem., Int. Ed.*, 2012, **51**, 10280–10283; (*b*) S. Guchhait, A. Khononov, T. Pienko, V. Belakhov and T. Baasov, *ACS Med. Chem. Lett.*, 2023, **14**, 794–801.

11 C. W. Bielawski and R. H. Grubbs, *Angew. Chem., Int. Ed.*, 2000, **39**, 2903–2906.

12 T. Singha, J. V. N. Kasu and D. P. Hari, *Angew. Chem., Int. Ed.*, 2025, **64**, e202505155.

13 (*a*) W. Yin and X. Wang, *New J. Chem.*, 2019, **43**, 3254–3264; (*b*) M. Szostak, M. Spain and D. J. Procter, *Angew. Chem., Int. Ed.*, 2013, **52**, 7237–7241; (*c*) L. Chen, Q. Qu, C. K. Ran, W. Wang, W. Zhang, Y. He and D. G. Yu, *Angew. Chem., Int. Ed.*, 2023, **62**, e202217918.

14 A. Bhunia and A. Studer, *Chem.*, 2021, **7**, 2060–2100.

15 (*a*) D. Q. Thach and R. R. Knowles, *Acc. Chem. Res.*, 2025, **58**, 2061–2071; (*b*) L. Chang, Q. An, L. Duan, K. Feng and Z. Zuo, *Chem. Rev.*, 2022, **122**, 2429–2486.

16 (*a*) A. Thanetchaiyakup, K. F. Chin, M. Dokic, P. M. L. Tan, D. J. Lin, M. Mathiew, X. Zhao, J. Z. X. Heng, D. J. X. Toh, X.-W. Liu, B. Ramalingam and H. S. Soo, *Chem Catal*, 2023,

Open Access Article. Published on 16 June 2026. Downloaded on 6/19/2026 2:50:40 PM. This article is licensed under a Creative Commons Attribution 3.0 Unported Licence.

3, 100530; (*b*) E. Tsui, H. Wang and R. R. Knowles, *Chem. Sci.*, 2020, **11**, 11124–11141.
17 (*a*) A. L. J. Beckwith and B. P. Hay, *J. Am. Chem. Soc.*, 1989, **111**, 230–234; (*b*) A. L. J. Beckwith and B. P. Hay, *J. Am. Chem. Soc.*, 1989, **111**, 2674–2681; (*c*) M. Bietti, O. Lanzalunga and M. Salamone, *J. Org. Chem.*, 2005, **70**, 1417–1422.
18 E. M. Dauncey, S. P. Morcillo, J. J. Douglas, N. S. Sheikh and D. Leonori, *Angew. Chem., Int. Ed.*, 2017, **57**, 744–748.
19 (*a*) K. Ouyang, W. Hao, W. X. Zhang and Z. Xi, *Chem. Rev.*, 2015, **115**, 12045–12090; (*b*) Q. Wang, Y. Su, L. Li and H. Huang, *Chem. Soc. Rev.*, 2016, **45**, 1257–1272.
20 (*a*) E. Ota and J. Yamaguchi, *Eur. J. Org. Chem.*, 2025, e202401322; (*b*) K. Aida, E. Ota and J. Yamaguchi, *Synthesis*, 2025, 2278–2288; (*c*) J. U. Kim, E. S. Lim, J. Y. Park, D. Jung and S. Lee, *Chem. Commun.*, 2025, **61**, 6997–7008.
21 (*a*) K. Aida, M. Hirao, T. Saitoh, T. Yamamoto, Y. Einaga, E. Ota and J. Yamaguchi, *J. Am. Chem. Soc.*, 2024, **146**, 30698–30707; (*b*) K. Aida, E. Ota and J. Yamaguchi, *Synlett*, 2025, 1142–1146.
22 T. Xiao, H. Huang, D. Anand and L. Zhou, *Synthesis*, 2020, 1585–1601.
23 (*a*) F. F. Fleming, *Nat. Prod. Rep.*, 1999, **16**, 597–606; (*b*) F. F. Fleming, L. Yao, P. C. Ravikumar, L. Funk and B. C. Shook, *J. Med. Chem.*, 2010, **53**, 7902–7917; (*c*) R. López and C. Palomo, *Angew. Chem., Int. Ed.*, 2015, **54**, 13170–13184.
24 (*a*) *Ullmann's Encyclopedia of Industrial Chemistry*, ed. B. Elvers, S. Hawkins and G. Schulz, Wiley-VCH, Weinheim, 2000; (*b*) H.-J. Arpe, *Industrielle Organische Chemie*, Wiley-VCH, Weinheim (Germany), 2007.
25 X. Wang, Y. Wang, X. Li, Z. Yu, C. Song and Y. Du, *RSC Med. Chem.*, 2021, **12**, 1650–1671.
26 (*a*) J. Boivin, A. C. Callier-Dublanchet, B. Quiclet-Sire, A.-M. Schiano and S. Z. Zard, *Tetrahedron*, 1995, **51**, 6517–6528; (*b*) M. F. Boselli, F. Medici and F. Franco, *SynOpen*, 2024, **8**, 273–299.
27 M. M. Jackman, S. Im, S. R. Bohman, C. C. L. Lo, A. L. Garrity and S. L. Castle, *Chem. Eur. J.*, 2018, **24**, 594–598.
28 J.-J. Zhang, X.-H. Duan, Y. Wu, J.-C. Yang and L.-N. Guo, *Chem. Sci.*, 2019, **10**, 161–166.
29 (*a*) W. Yuan, A. Qu, Y. Li, K. Chen and Y. Zhu, *Adv. Synth. Catal.*, 2022, **364**, 3932–3940; (*b*) P. J. Xia, Z. P. Ye, D. Song, H. Y. Xiang, X. Q. Chen and H. Yang, *Org. Lett.*, 2019, **21**, 2658–2662; (*c*) G. Han, J. You, J. Choi and E. J. Kang, *Org. Lett.*, 2024, **26**, 2414–2419.
30 M. A. Bryden, F. Millward, O. S. Lee, L. Cork, M. C. Gather, A. Steffen and E. Zysman-Colman, *Chem. Sci.*, 2024, **15**, 3741–3757.
31 J. Davies, S. G. Booth, S. Essafi, R. A. W. Dryfe and D. Leonori, *Angew. Chem., Int. Ed.*, 2015, **54**, 14017–14021.
32 L. Li, H. Chen, M. Mei and L. Zhou, *Chem. Commun.*, 2017, **53**, 11544–11547.
33 D. L. Zhang, Z. G. Le, Q. Li, Z. B. Xie, W. W. Yang and Z. Q. Zhu, *Chem. Commun.*, 2024, **60**, 2958–2961.
34 L. Chen, S. Jin, J. Gao, T. Liu, Y. Shao, J. Feng, K. Wang, T. Lu and D. Du, *Org. Lett.*, 2021, **23**, 394–399.
35 M. Lu, L. L. Jiang, Y. M. Xu, S. Li, Q. X. Tong and J. J. Zhong, *Chin. J. Chem.*, 2024, **42**, 2751–2756.
36 S. Kato, H. Nishiwaki, K. Endo and T. Hayashi, *Angew. Chem., Int. Ed.*, 2025, **64**, e202511590.
37 (*a*) T. Nishimura, T. Yoshinaka, Y. Nishiguchi, Y. Maeda and S. Uemura, *Org. Lett.*, 2005, **7**, 2425–2427; (*b*) H. B. Yang and N. Selander, *Chem. Eur. J.*, 2017, **23**, 1779–1783; (*c*) B. Zhao and Z. Shi, *Angew. Chem., Int. Ed.*, 2017, **56**, 12727–12731; (*d*) Y. R. Gu, X. H. Duan, L. Yang and L. N. Guo, *Org. Lett.*, 2017, **19**, 5908–5911.
38 X. Y. Yu, J. R. Chen, P. Z. Wang, M. N. Yang, D. Liang and W. J. Xiao, *Angew. Chem., Int. Ed.*, 2018, **57**, 738–743.
39 X. Shen, J. J. Zhao and S. Yu, *Org. Lett.*, 2018, **20**, 5523–5527.
40 B. Zhao, Y. Zheng, C. Chen, M. Wang, M. Ma and Z. Shi, *Org. Chem. Front.*, 2021, **8**, 2985–2989.
41 L. Tian, S. Gao, R. Wang, Y. Li, C. Tang, L. Shi and J. Fu, *Chem. Commun.*, 2019, **55**, 5347–5350.
42 B. Zhao, H. Tan, C. Chen, N. Jiao and Z. Shi, *Chin. J. Chem.*, 2018, **36**, 995–999.
43 B. Zhao, C. Chen, J. Lv, Z. Li, Y. Yuan and Z. Shi, *Org. Chem. Front.*, 2018, **5**, 2719–2722.
44 T. Guan, J. Y. Guo, Q. H. Zhang, X. W. Yu, X. Y. Yu, Y. Zhang and K. Zhao, *Green Chem.*, 2022, **24**, 6524–6530.
45 Y. Jian, M. Chen, C. Yang and W. Xia, *Eur. J. Org. Chem.*, 2020, 1439–1442.
46 H. C. Li, G. N. Li, H. S. Wang, Y. Tan, X. L. Chen and B. Yu, *Org. Chem. Front.*, 2024, **11**, 135–141.
47 C. Xiang, S. Yu, H. Fei, C. Pan and J. T. Yu, *Eur. J. Org. Chem.*, 2024, e202400245.
48 M. M. Zhang, S. H. Li, Q. Q. Min and F. Liu, *Org. Chem. Front.*, 2020, **7**, 622–627.
49 J. Chen, Y. J. Liang, P. Z. Wang, G. Q. Li, B. Zhang, H. Qian, X. D. Huan, W. Guan, W. J. Xiao and J. R. Chen, *J. Am. Chem. Soc.*, 2021, **143**, 13382–13392.
50 F. Le Vaillant, M. Garreau, S. Nicolai, G. Gryn'ova, C. Corminboeuf and J. Waser, *Chem. Sci.*, 2018, **9**, 5883–5889.
51 Y. He, D. Anand, Z. Sun and L. Zhou, *Org. Lett.*, 2019, **21**, 3769–3773.
52 P. Z. Wang, B. Q. He, Y. Cheng and W. J. Xiao, *Org. Lett.*, 2019, **21**, 6924–6929.
53 E. M. Dauncey, S. U. Dighe, J. J. Douglas and D. Leonori, *Chem. Sci.*, 2019, **10**, 7728–7733.
54 Z. Zhang, M. Li, W. Harrison, J. Lu, Z. Zhao, Y. Yuan and H. Zhao, *Nat. Catal.*, 2025, **8**, 548–555.
55 Y. Chen, J. Du and Z. Zuo, *Chem.*, 2020, **6**, 266–279.
56 R. J. Santen, H. Brodie, E. R. Simpson, P. K. Siiteri and A. Brodie, *Endocr. Rev.*, 2009, **30**, 343–375.
57 R. B. King and A. Efraty, *J. Am. Chem. Soc.*, 1972, **94**, 3773–3779.
58 (*a*) R. H. Crabtree, R. P. Dion, D. J. Gibboni, D. V. McGrath and E. M. Holt, *J. Am. Chem. Soc.*, 1986, **108**, 7222–7227; (*b*) M. A. Halcrow, F. Urbanos and B. Chaudret,

Open Access Article. Published on 16 June 2026. Downloaded on 6/19/2026 2:50:40 PM. This article is licensed under a Creative Commons Attribution 3.0 Unported Licence.

Organometallics, 1993, **12**, 955–957; (*c*) S. W. Youn, B. S. Kim and A. R. Jagdale, *J. Am. Chem. Soc.*, 2012, **134**, 11308–11311; (*d*) G. Smits, B. Audic, M. D. Wodrich, C. Corminboeuf and N. Cramer, *Chem. Sci.*, 2017, **8**, 7174–7179.

59 (*a*) P. P. Mondal, A. Pal, A. K. Prakash and B. Sahoo, *Chem. Commun.*, 2022, **58**, 13202–13205; (*b*) X.-Y. Lv, R. Abrams and R. Martin, *Angew. Chem., Int. Ed.*, 2023, **62**, e202217386.

60 L. Li, L. Fang, W. Wu and J. Zhu, *Org. Lett.*, 2020, **22**, 5401–5406.

61 H.-J. Miao, J.-H. Zhang, W. Li, W. Yang, H. Xin, P. Gao, X.-H. Duan and L.-N. Guo, *Chem. Sci.*, 2024, **15**, 8993–8999.

62 J.-H. Zhang, H.-J. Miao, J.-Y. Li, W. Li, P. Ma, X.-H. Duan and L.-N. Guo, *Chem. Commun.*, 2024, **60**, 8095–8098.

63 W.-P. Yang, H.-J. Miao, L. Liu, X. H. Duan and L.-N. Guo, *Org. Lett.*, 2024, **26**, 7442–7446.

64 W. Li, H.-J. Miao, J.-H. Zhang, X.-H. Duan and L.-N. Guo, *Chem. Eur. J.*, 2024, **30**, e202402602.

65 W.-P. Yang, H.-J. Miao, G. Wang, X. Yang, X. Wang, L. Liu, X.-H. Duan and L.-N. Guo, *J. Org. Chem.*, 2024, **89**, 18713–18722.

66 J. W. Zhang, Y. R. Wang, J. H. Pan, Y. H. He, W. Yu and B. Han, *Angew. Chem., Int. Ed.*, 2020, **59**, 3900–3904.

67 E. Vitaku, D. T. Smith and J. T. Njardarson, *J. Med. Chem.*, 2014, **57**, 10257–10274.

68 X. Zhou, Y. Xu and G. Dong, *J. Am. Chem. Soc.*, 2021, **143**, 20042–20048.

69 X. Zhou, T. Yu and G. Dong, *J. Am. Chem. Soc.*, 2022, **144**, 9570–9575.

70 X. Zhou, D. Pyle, Z. Zhang and G. Dong, *Angew. Chem., Int. Ed.*, 2023, **62**, e202213691.

71 Z. Zhang, Q. Zhu, D. Pyle, X. Zhou and G. Dong, *J. Am. Chem. Soc.*, 2023, **145**, 21096–21103.

72 X. Zhou, Y. Xu and G. Dong, *Nat. Catal.*, 2021, **4**, 703–710.

73 B. Zhang, H. Bai, B. Zhan, K. Wei, S. Nie and X. Zhang, *Sci. Adv.*, 2024, **10**, eado0225.

74 (*a*) A. Lin, S. Lee and R. R. Knowles, *Acc. Chem. Res.*, 2024, **57**, 1827–1838; (*b*) Q. An, L. Chang, H. Pan and Z. Zuo, *Acc. Chem. Res.*, 2024, **57**(19), 2915–2927.

75 (*a*) M. H. V. Huynh and T. J. Meyer, *Chem. Rev.*, 2007, **107**, 5004–5064; (*b*) B. L. Greene, C.-H. Wu, G. E. Vansuch, M. W. W. Adams and R. B. Dyer, *Biochemistry*, 2016, **55**, 1813–1825.

76 (*a*) C. Costentin, D. H. Evans, M. Robert, J.-M. Savéant and P. S. Singh, *J. Am. Chem. Soc.*, 2005, **127**, 12490; (*b*) J. J. Warren, T. A. Tronic and J. M. Mayer, *Chem. Rev.*, 2010, **110**, 6961–7001.

77 R. G. Agarwal, S. C. Coste, B. D. Groff, A. M. Heuer, H. Noh, G. A. Parada, C. F. Wise, E. M. Nichols, J. J. Warren and J. M. Mayer, *Chem. Rev.*, 2022, **122**, 1–49.

78 P. R. D. Murray, J. H. Cox, N. D. Chiappini, C. B. Roos, E. A. McLoughlin, B. G. Hejna, S. T. Nguyen, H. H. Ripberger, J. M. Ganley, E. Tsui, N. Y. Shin, B. Koronkiewicz, G. Qiu and R. R. Knowles, *Chem. Rev.*, 2022, **122**, 2017–2291.

79 H. G. Yayla, H. Wang, K. T. Tarantino, H. S. Orbe and R. R. Knowles, *J. Am. Chem. Soc.*, 2016, **138**, 10794–10797.

80 E. Ota, H. Wang, N. L. Frye and R. R. Knowles, *J. Am. Chem. Soc.*, 2019, **141**, 1457–1462.

81 D. Wang, J. Mao and C. Zhu, *Chem. Sci.*, 2018, **9**, 5805–5809.

82 T. Ji, X.-Y. Chen, L. Huang and M. Rueping, *Org. Lett.*, 2020, **22**, 2579–2583.

83 R. Hua, Q. Wang, H. Yin and F.-X. Chen, *Chem. Eur. J.*, 2024, **30**, e202400453.

84 J. Wang, B. Huang, C. Shi, C. Yang and W. Xia, *J. Org. Chem.*, 2018, **83**, 9696–9706.

85 J. Tian, Z. Sun, W. Li, D. Wang and L. Zhou, *New J. Chem.*, 2022, **46**, 8545–8550.

86 X. Wang, Y. Li, J. Zhang and X. Wu, *Mol. Catal.*, 2022, **533**, 112788.

87 W. Zeng, X. Zhang, Y. Zhang, S. Xiao, Y. Tang, P. Xie and T.-P. Loh, *Org. Lett.*, 2023, **25**, 5869–5874.

88 N. Salaverri, B. Carli, P. B. Gratal, L. Marzo and J. Alemán, *Adv. Synth. Catal.*, 2022, **364**, 1689–1694.

89 R. Chowdhury, A. K. Dubey and R. Ghosh, *J. Org. Chem.*, 2024, **89**(10), 7187–7200.

90 N. Salaverri, B. Carli, S. Díaz-Tendero, L. Marzo and J. Alemán, *Org. Lett.*, 2022, **24**, 3123–3127.

91 B. Carli, N. Salaverri, L. Martínez-Fernández, M. Goicuría, J. Alemán and L. Marzo, *Org. Lett.*, 2024, **26**, 4542–4547.

92 (*a*) S. Wu, J. Li, R. He, K. Jia and Y. Chen, *Org. Lett.*, 2021, **23**, 9204–9209; (*b*) L. Huang, T. Ji, C. Zhu, H. Yue, N. Zhumabay and M. Rueping, *Nat. Commun.*, 2022, **13**, 809.

93 X. Wang, Y. Li and X. Wu, *ACS Catal.*, 2022, **12**, 3710–3718.

94 B. Wang, H. Li, L. Wang, Y.-G. Liu and J. Wu, *Chem. Catal.*, 2022, **2**, 2096–2105.

95 L. Huang, T. Ji and M. Rueping, *J. Am. Chem. Soc.*, 2020, **142**, 3532–3539.

96 T.-T. Zhao, W.-L. Yu, Z. T. Feng, H.-N. Qin, H.-X. Zheng and P.-F. Xu, *Chem. Commun.*, 2022, **58**, 1171–1174.

97 H. Keum, H. Ryoo, D. Kim and S. Chang, *J. Am. Chem. Soc.*, 2024, **146**(1), 1001–1008.

98 J. Cao, C. R. Schull and K. A. Scheit, *Angew. Chem., Int. Ed.*, 2025, **137**, e202507542.

99 Y. Ao, N. Wang, S.-Y. Tang, Z.-J. Wang, L.-H. Zou and H.-M. Huang, *ACS Catal.*, 2025, **15**, 2212–2221.

100 F. Juliá, *ChemCatChem*, 2022, **14**, e202200916.

101 J.-J. Guo, A. Hu, Y. Chen, J. Sun, H. Tang and Z. Zuo, *Angew. Chem., Int. Ed.*, 2016, **55**, 15319–15322.

102 A. Hu, Y. Chen, J.-J. Guo, N. Yu, Q. An and Z. Zuo, *J. Am. Chem. Soc.*, 2018, **140**, 13580–13585.

103 A. O. Morris and L. Barriault, *Chem. Eur. J.*, 2024, **30**, e202400642.

104 W. Liu, Q. Wu, M. Wang, Y. Huang and P. Hu, *Org. Lett.*, 2021, **23**, 8413–8418.

105 Q. Wu, W. Liu, M. Wang, Y. Huang and P. Hu, *Chem. Commun.*, 2022, **58**, 9886–9889.

106 K. Wang and R. Zeng, *Org. Chem. Front.*, 2022, **9**, 3692–3696.

 This journal is © The Royal Society of Chemistry 2026

Open Access Article. Published on 16 June 2026. Downloaded on 6/19/2026 2:50:40 PM.
This article is licensed under a Creative Commons Attribution 3.0 Unported Licence.

107 Z. Zhang, T. Xue, Z. Han and R. Zeng, *Synthesis*, 2023, 433–442.
108 S. Gazi, W. K. H. Ng, R. Ganguly, A. M. P. Moeljadi, H. Hirao and H. S. Soo, *Chem. Sci.*, 2015, **6**, 7130–7142.
109 L. Wen, J. Ding, L. Duan, S. Wang, Q. An, H. Wang and Z. Zuo, *Science*, 2023, **382**, 458–464.
110 Z. Yang, D. Yang, J. Zhang, C. Tan, J. Li, S. Wang, H. Zhang, Z. Huang and A. Lei, *J. Am. Chem. Soc.*, 2022, **144**, 13895–13902.
111 (*a*) H. Wang, Z. Chen, J. Fan, G. Liang, Q. He and D. Zhang, *Org. Lett.*, 2025, **27**, 10968–10973; (*b*) M. A. Bashir, Y. Jiang, C.-H. Hu, Z. Lin and C. Zhu, *Org. Lett.*, 2025, **27**, 12980–12985.
112 M. Jaber, Y. Ozbay, E. Chefdeville, G. Tran and A. Amgoune, *ACS Catal.*, 2024, **14**, 12757–12768.
113 L. Zou, R. Sun, Y. Tao, X. Wang, X. Zheng and Q. Lu, *Nat. Commun.*, 2024, **15**, 5245.
114 Z.-R. Liu, X.-Y. Zhu, J.-F. Guo, C. Ma, Z. Zuo and T.-S. Mei, *Sci. Bull.*, 2024, **69**, 1866–1874.
115 M. Pramanik and R. L. Melen, *Chem*, 2023, **9**, 2060–2062.
116 M. Ju, S. Lee, H. M. Marvich and S. Lin, *J. Am. Chem. Soc.*, 2024, **146**, 19696–19703.
117 C. R. Pitts, M. S. Bloom, D. D. Bume, Q. A. Zhang and T. Lectka, *Chem. Sci.*, 2015, **6**, 5225–5229.
118 J. L. Tu, H. Gao, M. Luo, L. Zhao, C. Yang, L. Guo and W. Xia, *Green Chem.*, 2022, **24**, 5553–5558.
119 K. Zhang, J. Wang, W. Chen, M. Li, S. Jin and Z. Zuo, *Green Chem.*, 2025, **27**, 1023–1030.
120 Y. Xu, W. Chen, R. Pu, J. Ding, Q. An, Y. Yang, W. Liu and Z. Zuo, *Nat. Commun.*, 2024, **15**, 9366.
121 (*a*) H.-J. Miao, J.-H. Zhang, S. Liu, W. H. Wang, X. Yang, X.-H. Duan and L.-N. Guo, *Org. Lett.*, 2023, **25**, 5563–5568; (*b*) S. Liu, P. Ma, L. Zhang, S. Shen, H.-J. Miao, L. Liu, K. N. Houk, X.-H. Duan and L.-N. Guo, *Chem. Sci.*, 2023, **14**, 5220–5225; (*c*) J.-Q. Tao, S. Liu, T.-Y. Zhang, H. Xin, X. Yang, X.-H. Duan and L.-N. Guo, *Chin. Chem. Lett.*, 2024, **35**, 109263; (*d*) M. Dang, R. Jia, K. Tan, D. Hao, W. Yang, C.-Y. Zhou and Z. Guo, *J. Org. Chem.*, 2024, **89**, 4031–4036.
122 J. Du, X. Yang, X. Wang, Q. An, X. He, H. Pan and Z. Zuo, *Angew. Chem., Int. Ed.*, 2021, **60**, 5370–5376.
123 (*a*) L. Chen, L.-N. Guo, S. Liu, L. Liu and X.-H. Duan, *Chem. Sci.*, 2021, **12**, 1791–1795; (*b*) T. Singha, G. A. Kadam and D. P. Hari, *Chem. Sci.*, 2023, **14**, 6930–6935.
124 D. Q. Thach and R. R. Knowles, *J. Am. Chem. Soc.*, 2025, **147**, 21818–21823.
125 S. F. Kim, H. Schwarz, J. Jurczyk, B. R. Nebgen, H. Hendricks, H. Park, A. Radosevich, M. W. Zuerch, K. Harper, M. C. Lux, C. S. Yeung and R. Sarpong, *J. Am. Chem. Soc.*, 2024, **146**, 5580–5596.
126 S. F. Kim, J. P. Liles, M. C. Lux, H. Park, J. Jurczyk, Y. Soda, C. S. Yeung, M. S. Sigman and R. Sarpong, *J. Am. Chem. Soc.*, 2025, **147**, 1851–1866.
127 J. Woo, A. H. Christian, S. A. Burguer, Y. Jiang, U. F. Mansoor and M. D. Levin, *Science*, 2022, **376**, 527–532.